

Ceramics from Khalet al-Jam'a (Bethlehem, Palestine): a material hidden for millennia

Laureando
Yun-Wen Liao

Relatore
Laura Medeghini



SAPIENZA
UNIVERSITÀ DI ROMA



UNIVERSIDADE
DE ÉVORA



Erasmus Mundus Joint Master in
ARChaeological MATerials Science



SAPIENZA
UNIVERSITÀ DI ROMA



UNIVERSIDADE
DE ÉVORA



Erasmus Mundus Joint Master in
ARChaeological MATerials Science

Ceramics from Khalet al-Jam'a (Bethlehem, Palestine): a material hidden for millennia

Facoltà di Scienze Matematiche, Fisiche e Naturali
Dipartimento di Biologia Ambientale
Corso di laurea in Scienze e Tecnologie per la Conservazione dei Beni Culturali

Yun-Wen Liao
Matricola 1873932

Relatore
Laura Medeghini

Correlatore
Michela Botticelli

A.A. 0000-0000

Ceramics from Khalet al-Jam'a (Bethlehem, Palestine):
a material hidden for millennia

1. Introduction
2. Ceramic
 - 2.1 Definition
 - 2.2 History
 - 2.3 Main Components
 - 2.4 Ceramic Types
 - 2.4.1 Earthenware
 - 2.4.2 Stoneware
 - 2.4.3 Porcelain
3. Archaeological Setting
 - 3.1 About the Site
 - 3.2 Archaeological Phases
 - 3.3 Materials Found in the Site
4. Geological Setting
5. Materials and methods
 - 5.1 Samples
 - 5.2 Experimental
 - 5.2.1 Optical Microscopy
 - 5.2.2 X-ray Diffraction
 - 5.2.3 Scanning Electron Microscopy coupled with Energy Dispersive Spectroscopy
6. Results
 - 6.1 Optical microscopy analysis (OM)
 - 6.2 X-ray Diffraction analysis (XRD)
 - 6.3 Scanning Electron Microscopy coupled with Energy Dispersive Spectroscopy (SEM-EDS)
7. Discussion
 - 7.1 Technological level
 - 7.1.1 Nature of the raw material
 - 7.1.2 Firing conditions
 - 7.2 Provenance
 - 7.3 Burial conditions
8. Conclusions

References

Acknowledgement

Chapter 1 Introduction

Bethlehem, the ancient city of Palestine, has been known for its religious and historical significance for millennia. A recently excavated site, Khalet al-Jam'a, was unearthed and surveyed by a joint team of the Palestinian MOTA-DACH (Ministry of Tourism and Antiquities - Department of Archaeology and Cultural Heritage) and Sapienza University of Rome in 2013-2016 and abundant materials were recovered.

This study is focused on the mineralogical-petrographic and chemical characterization of ceramic material yielded from this site, with the aim to reconstruct the technological level reached by the ancient civilization occupying it during the Early Bronze Age. Optical microscopy (OM), X-ray Powder Diffraction (XRPD) and Scanning Electron Microscopy with Energy Dispersive X-ray Spectroscopy (SEM-EDS) provided results which can define the nature and provenance of raw materials, as well as technological aspects such as firing conditions and post-burial processes, to finally give a view of the socio-economic status at that time.

Chapter 2 Ceramic

2.1 Definition

Ancient pottery, also termed as ceramics or ceramic art, denotes the creation of objects made primarily out of clays, which are hardened with heat to increase their strength and solidity and give them a chemically resistant, durable form (Sinopoli, 1991). Pottery was mostly shaped in vessels, plates or bowls for the purpose of cooking or storage. The excellent durability and relative abundance make it survive for even millennia. Ceramics and the sherds are the most common and typically found items in archaeological sites, which are significant indicators of social and economic development for understanding the past (Meyer *et al.*, 2016).

2.2 History

The main component of ceramics is the clay, which is abundant, easily accessible, flexible during production and could be fired to enhance the strength. These features drove the invention and development of ceramics in the birth of civilizations.

As one of the oldest human functional art to emerge during the period prior to the Neolithic, the earliest appearance dates back to the 29,000–25,000 BC: fired and unfired clay figurines were found in the Dolni Vestonice site in Czech Republic (Vandiver *et al.*, 1989). These ceramics were made of clay material and animal fat and bone/bone ash mixed, fired at a low temperature range of 500-800 °C. Several thousand years later shaped pottery vessels emerged in Xianrendong Cave in Jiangxi, China, dated back to 18,000 BC and spread to Japan and the Russian Far East region. Early Neolithic ceramics were also found in Jōmon, Japan (Diamond, 1998), which were dated as early as 14,500 BC (Selkirk, 2003). Interestingly, the word “Jōmon” is “cord-marked” in Japanese, representing the marking of pottery and ceramic figures by the use of sticks with cords for decoration before firing. Other ancient ceramics emerged independently across various regions: during the 10th millennium BC in Sub-Saharan Africa (Huysecom *et al.*, 2009), and in South America during the 10,000 BC (Silla, 1997).

In the wake of raising of settled communities and dedicating to agriculture and farming, the changed lifestyle induced the utilization and development of ceramics during the Neolithic period. The flourish of ceramics began in around 9000 BC. Besides serving

as container, ceramics also came out as art objects, tiles and bricks, spreading from Asia to the Middle East and Europe (Meyer *et al.*, 2016).

Another worth mentioning breakthrough happened around 6000 to 4000 BC, the invention of the potter's wheel was considered to be the most significant development in the history of pottery (Kramer, 2010). This revolutionized the production of uniform and refined shapes.

Playing an important role in ancient times and in various cultures, the technology and application of ceramics kept developing and progressing, reaching its full potential nowadays.

2.3 Main Components

Ceramics are composed of several substances. They are clay minerals, minerals and sometimes accidental materials. Mixing with appropriate additives and water, clay minerals could be plastic and be shaped into any desired forms when they are wet and could retain the shape without deforming throughout the firing process. Coming from weathering and decomposition of silicate rocks or sedimentary processes, clay minerals are sheet (layered) silicates. They are structurally built of sheets of tetrahedral silicon dioxide (SiO_2) and octahedral aluminium oxide (Al_2O_3) linked through bridging oxygen atoms, and categorized by the features of layered type. Kaolinite, illite and montmorillonite are common clay minerals (Nesse, 2012).

Clay minerals are built of tetrahedral silicate (T) sheets and octahedral hydroxide sheets (O) (Fig. 1). The tetrahedron consists of one atom of silicon (or aluminum) in the center and 4 atoms of oxygen in the vertexes of the tetrahedron, while the octahedron is made of one atom of aluminum (or magnesium, or iron) in the center and 6 OH groups in the vertexes (Grim, 1962).

Amongst these, kaolinite ($\text{Al}_2\text{Si}_2\text{O}_5(\text{OH})_4$), the most widely and extensively used clay mineral, usually comes from chemical weathering of feldspars or other aluminum silicate minerals (Nesse, 2012). It is soft and earthy, with a layered structure made of one tetrahedral sheet of silica linked through oxygen atoms to one octahedral sheet of alumina (TO structure), having weak van der Waals bonds between T-O groups. The structure gives it properties such as a low shrink–swell capacity and leads to transformations during ceramics making, especially upon thermal treatment.

Illite has about one-sixth of silicon replaced by aluminum, resulting in a charge deficiency compensated by potassium ions, or by Ca^{2+} , Mg^{2+} and H. The given chemical formula is $(\text{K}, \text{H}_3\text{O})(\text{Al}, \text{Mg}, \text{Fe})_2(\text{Si}, \text{Al})_4\text{O}_{10}[(\text{OH})_2, (\text{H}_2\text{O})]$ and the structure is a 2:1 sandwich of silica tetrahedron (T) – alumina octahedron (O) – silica tetrahedron

(T), TOT layers. It is a weathering or hydrothermal alteration of muscovite or feldspar, commonly found in marine deposits (Nesse, 2012).

Montmorillonite, belongs to the smectite clays, has a structure that two tetrahedral sheets of silica sandwiching a central octahedral sheet of alumina (TOT). Its crystals are relatively loosely bound and allow water to intervene, making the clay to swell (Nesse, 2012).

Common minerals in ceramics are also quartz, K-feldspar, plagioclase, mica, clinopyroxene, amphibole, olivine, calcite and iron oxide. Accidental materials could be organic materials, fragments of rocks and fossils.

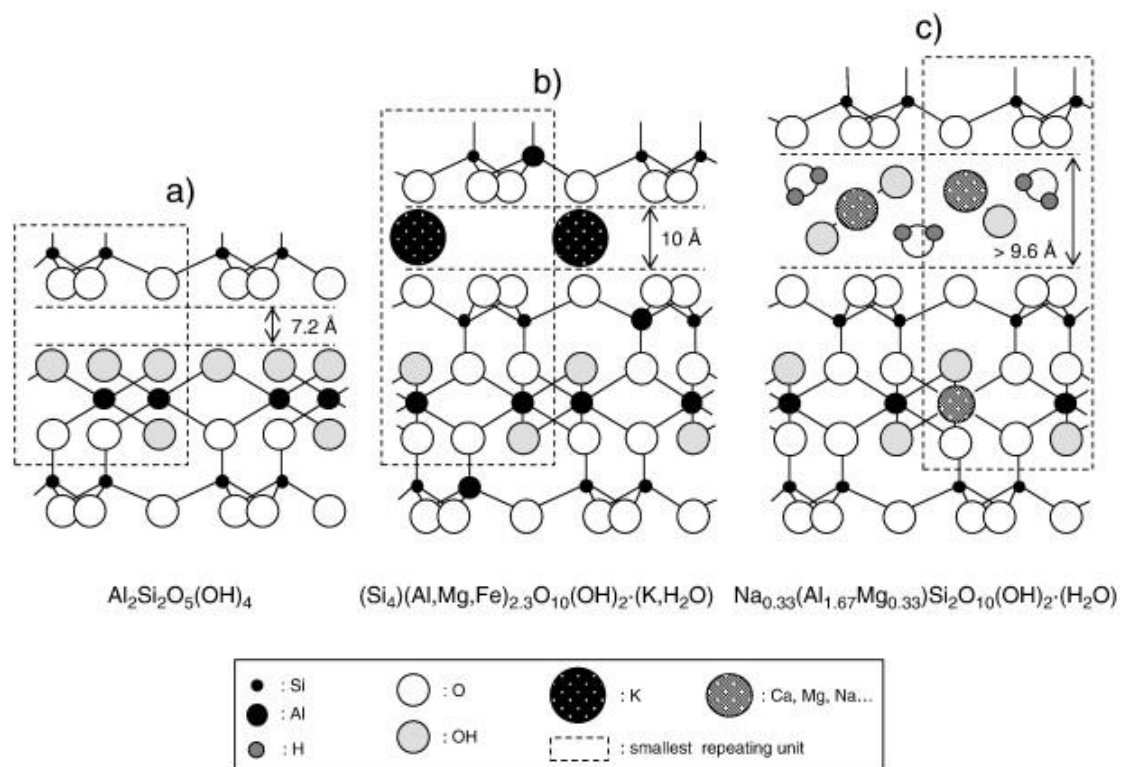


Fig. 1 Structures and empirical formulas of kaolinite (a), illite (b) and montmorillonite (c) (Grim, 1962)

Besides clays, non-plastic material, *i.e.* tempers, are added to improve the strength and to reduce the plasticity of the clay, for the purpose of preventing potential shrinkage and cracking during drying and firing. They also serve as a flux agent to lower the firing temperature (Nesse, 2012).

2.4 Ceramic Types

Clay-based ceramics could be divided into 3 major categories: earthenware, stoneware and porcelain.

2.4.1 Earthenware

Earthenware (Figs. 2,3) is the basic type amongst these categories, normally fired around 800-1100 °C and more or less unvitriified and coarser than other kinds of ceramics. It is porous and water-permeable, usually with high proportion of non-plastic constituents which give it high degree of porosity. It has lower mechanical strength and sometimes a flux like calcium oxide is added to increase its durability. Earthenware could be completely or decorated slipped. In the case of improving its impermeability for liquid storage due to porosity, a glaze would be applied to the surface, the bonding to the body being usually weak and appearing distinct in cross-section. Most of the oldest ancient ceramics, *i.e.* the wares of Egypt, Persia and the near East; Greek, Roman, and up to medieval, European painted ceramics, even some Chinese ceramics, are earthenware.

The term "Terracotta" (Reedy, 2008), showed in Figure 4, is used for referring the low-fired unglazed clay bodies being fired to red or cream. This word could also refer to non-pottery ceramics, for example sculpture made in earthenware, or objects not made on a potter's wheel.

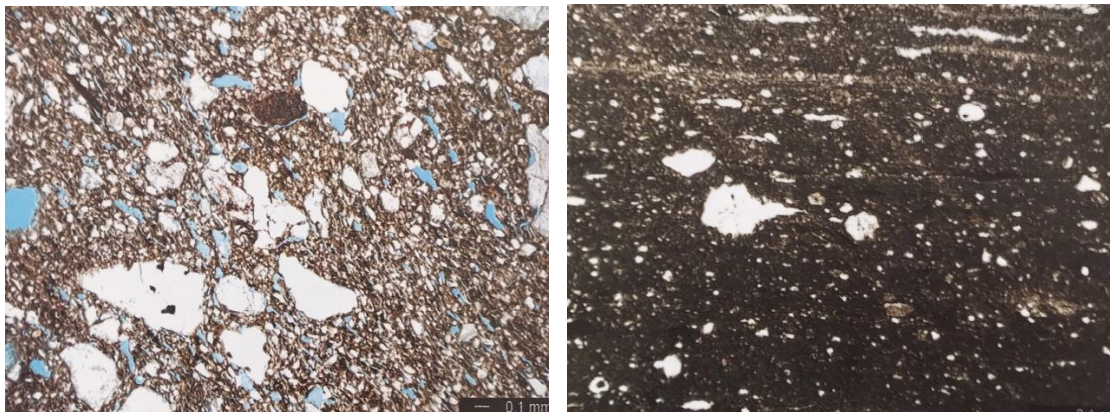


Fig. 2 Earthenware, plane polarized light.

This kind of low-fired earthenware tend to present high content of non-plastic constituents, either natural or deliberately added, which lead to a high porosity (Reedy, 2008).

Figure. 3 Earthenware with a more intermediate firing temperature, plane polarized light. It is denser and partially vitrified, having less porosity (Reedy, 2008).

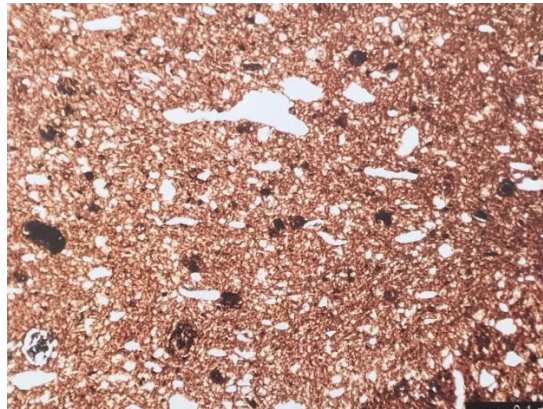


Fig. 4 Terracotta under plane polarized light. It tends to be rather porous and coarse. Deep reddish to black chunks of hematite and elongated pores could be seen (Reedy, 2008).

2.4.2 Stoneware

The denser, more durable stoneware (Figs. 5,6) is fired at relatively higher temperature, between 1100 and 1300 °C. The temperature is high enough to allow the vitrification start, thus the stoneware is more vitrified, denser, stronger as well as improved in terms of impermeability to water. The fusibility is also enhanced when they are glazed. They display several colours, for example off white, gray, cream, tan or light brown. Raw materials include mainly clay, micas, feldspars and quartz, with fewer iron oxide minerals compared to earthenware and thus give stonewares lighter in colour. Ancient stoneware dates back to Bronze Age in the northwestern regions of South Asia, and few centuries later developed into more considerable quantities (Reedy, 2008)



Fig. 5 Stoneware under plane polarized light. The comparatively dense material of this stoneware consists of a clay matrix which is partially vitrified (Reedy, 2008).

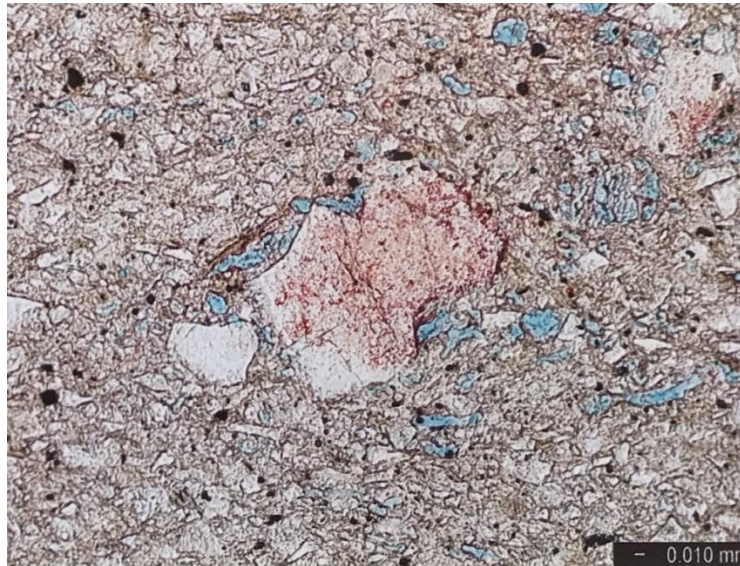


Fig. 6 An example of lower fired stoneware under plane polarized light. Some large grains of feldspar are visible- the red stain helps to identify plagioclase feldspar, while the blue areas are voids. Some fine-grained tabular brown micas (chlorite) are also present in the clay matrix, along with the scattered black grains of magnetite (Reedy, 2008).

2.4.3 Porcelain

Porcelain comes from a refined clay which is fired at very high temperature (it achieve 1200 to 1450 °C). Reaching such high temperature, the high degree of vitrification and the formation of the mineral mullite result in toughness, strength, and translucence in appearance (Reedy, 2008). Out of the main three types of ceramics, porcelain owns the prestige of its delicacy, strength, and the beautiful white colour (Fig. 7). It came out first in China and the technique of production achieved mature around 2000 to 1200 years ago (Chen, 2004) and spread to East Asia and Europe. However, the mastering of porcelain was found to be achieved until the 18th century in Meissen, Germany (Finlay, 1998).

They could be further categorized into some sub-types: hard-paste, soft-paste and bone china, stone paste/fritware, according to the firing conditions and the composition of the paste of the body (Reedy, 2008). Hard-paste porcelain, also called “true porcelain”, is made from naturally occurring materials and fired at higher temperature, usually around 1400°C (Rado, 1988). Soft-paste type is differentiated from the former by a lower firing temperature around 1200°C and the involvement of some synthetic ingredients. Its body is more granular than hard-paste type and lee glass formed in firing process. Because of the introduction of bone ash serving as a flux into the clay, bone china is strong and dense, especially known for its high levels of off-white colour and translucency. The fritware consists of crushed quartz combined with small amount of very plastic clay and alkaline crushed glass frit, where the frit is added to clay in the purpose of reducing the fusion temperature. It is known and extensively used in the Islamic world (Rado, 1988).

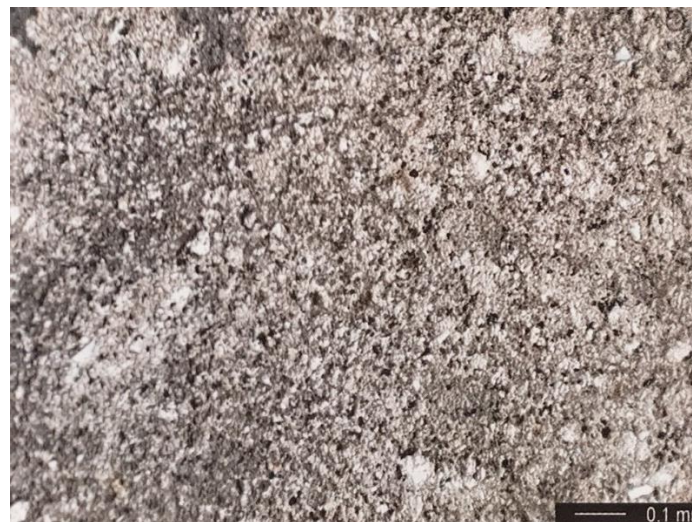


Fig. 7 Porcelain (hard paste), plane polarized light. This example is from a modern Korean porcelain piece and the high dense characteristic made the epoxy barely be seen (Reedy, 2008).

Chapter 3 Archaeological Setting

3.1 About the Site

The Khalet al-Jam'a site was first reported for the retrieval of a rock-cut tomb to the MOTA-DACH Office of Bethlehem during the construction of an industrial park in spring 2013. It is located 2.2 Km south-east away from the centre of Bethlehem, on the south-eastern slope of the hill of Hindaza (Fig. 8). Archaeologists in Palestine preliminarily recovered some items and later identified multi-period necropolis. Undergoing a series of rescue excavations undertaken by the joint team of the Palestinian MOTA-DACH and Sapienza University of Rome, the site was identified as funerary area where different historical phases coexist, dated back to Intermediate Bronze Age (EB IV), Middle Bronze Age (MB) and through the whole Iron Age (Nigro *et al.*, 2018).

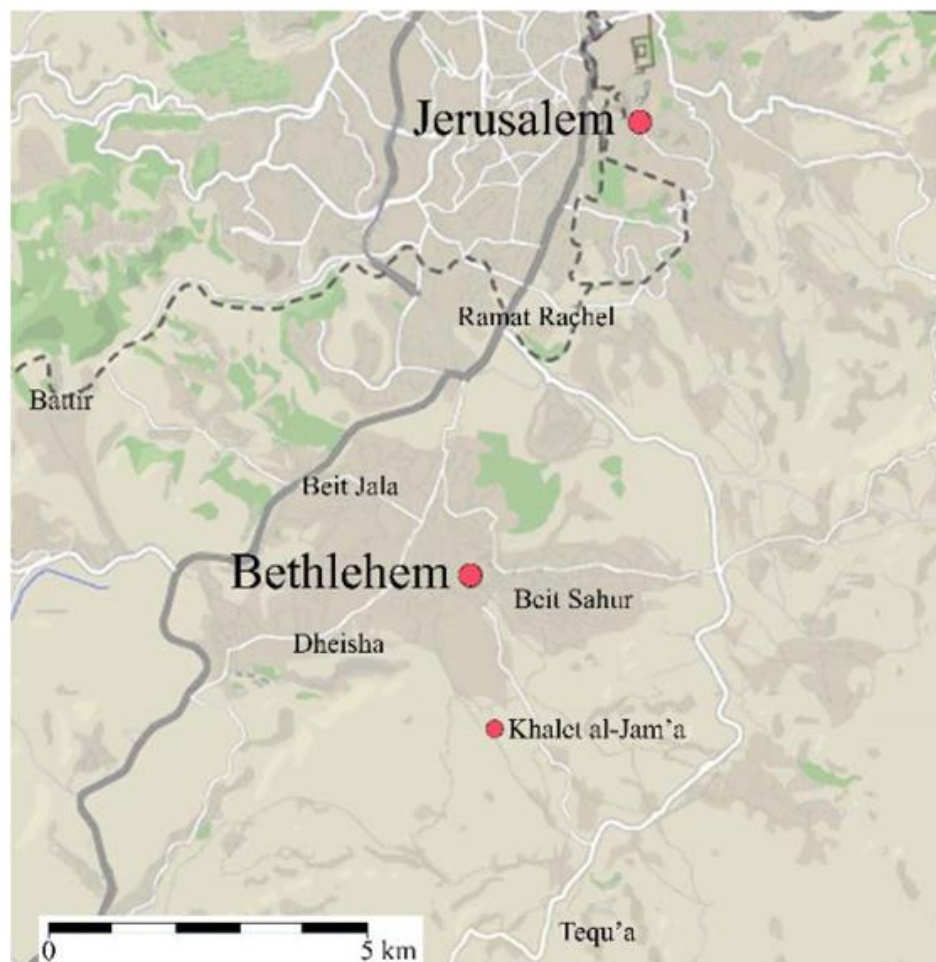


Fig. 8 Location map of the Bethlehem city and the Khalet al-Jam'a site (Nigro *et al.*, 2018).

3.2 Archaeological Phases

From the sketch map of satellite photo (Fig. 9), the exploitation was revealed using the natural characteristics of the bedrock emerging in series of sloping terraces. The largest Intermediate Bronze Age (EB IV)-Middle Bronze I-III cemetery is situated on the lower southernmost terrace, while a less densely exploited Iron Age cemetery was embedded on the upper northernmost terrace. Some erected modern buildings partially wrecked the upper cemetery and only a few tombs survived on the top of the Hindaza hill. Luckily, the lower cemetery persisted and was cleared off for at least two thirds of its original extension, so that at least 30 tombs were identified.



Fig. 9 Sketch map of Khalet al-Jam'a necropolis overlying a satellite photo (Nigro *et al.*, 2018).

The site was divided into four areas termed A, B, C and D (Fig. 10), according to its topography. The upper northern terrace of the MB cemetery, denoted as Area A, only preserved its western side; Area B indicates the lower south-eastern quadrant of the same cemetery; Area C includes the sloping south-western quadrant of the MB cemetery, and the northern cemetery was assigned to be Area D. A rock step marks the boundary between the northern and southern cemeteries (Nigro *et al.*, 2018).

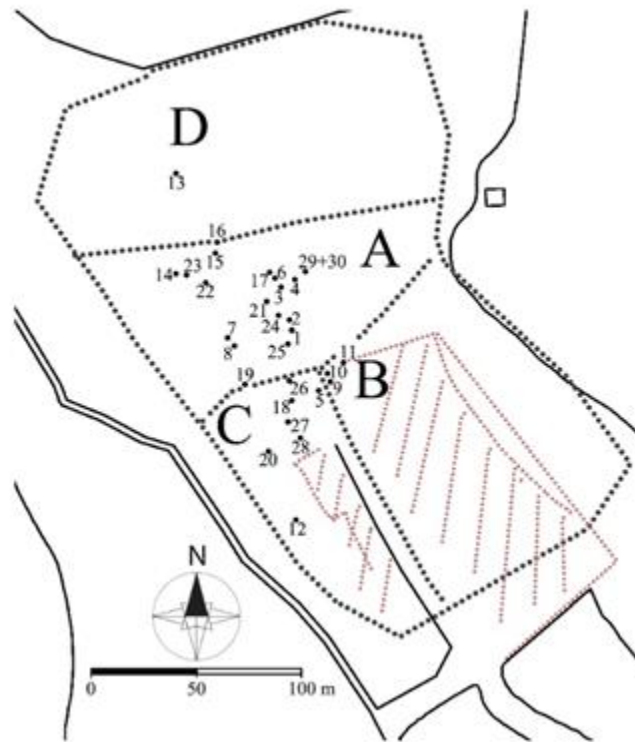


Fig. 10 Plan of the necropolis with subdivision in areas and tombs (Nigro *et al.*, 2018).

3.2.1 The necropolis

3.2.1.1 Area A - the Middle Bronze cemetery on the north-western terrace

The preliminary survey has identified Area A as a Middle Bronze cemetery with nineteen tombs distributed in the central and western sectors. Five tombs (Tombs A1, A2, A3, A4, A6) were first excavated by MOTA-DACH; Tomb A7, A8 were also identified and protected; other five tombs (Tombs A14, A15, A16, A17, A19) were found already looted and only a few items were yielded from them. Later in the survey of May 2015, five more tombs (A22, A23, A24, A25, A26) were recognized and the last two tombs (A29 and A30) were regrettably removed by the bulldozer, and only their cut shafts remained clear (Nigro *et al.*, 2018).

3.2.1.2 Area B - the Middle Bronze cemetery

Located in the south-eastern sector of the necropolis, Area B is demarcated by the road of the factory area to the west and by the modern road climbing towards the modern water tower to the east. This area is badly damaged by the building and it was

speculated that at least two dozens of tombs were completely eliminated. Thus, the excavation only yielded three tombs, B9, B10, B11 at the north-west corner of the Area (Nigro *et al.*, 2018).

3.2.1.3 Area C - the Intermediate Bronze Age/Early Bronze IV cemetery

The south-western sector is denoted as Area C. The MOTA-DACH excavated two tombs, C5 and C12 in the rescue activity. There were two tombs, C18 and C20, unfortunately already looted. The rest three tombs, C26, C27 and C28 were identified in the north-central zone of the area. They probably belong to the MB cemetery (Nigro *et al.*, 2018).

3.2.1.4 Area D

The most northern terrace was denoted as Area D, which is a later expansion of the necropolis. Due to the construction, only one tomb was discovered and named Barmils' Tomb (Tomb D13). From the ceramics and personal ornaments yielded, it is presumed that the tomb dates back from Iron IB to Iron IIC (Nigro *et al.*, 2018).

3.2.2 Built up installations in the necropolis area

Interestingly, some built up installations were also found in the necropolis area, which indicate the long-lasting occupation of the south-eastern flank of the Hindaza hill (Fig. 11).

For example, a rock-cut wine press was found, consisting of a large pressing vat, 2.5 x 2.7 m, carved out in the bedrock and connected via short channels with two other smaller square basins. This wine press was supposed to come from the Byzantine Period. The three rock-cut vats were plastered with a pinkish hydraulic revetment of 1.2 cm thickness. A couple of round installations were also found connected with wine production in the southeast of these two square basins. In the northern part of Tomb A7, two circular stone-built lime kilns were recovered, which also date to the Byzantine Period. Close to the tomb and roughly at the centre of the lower terrace, the limestone boulder foundations of an Iron Age tower were unearthed as well (Nigro *et al.*, 2018).

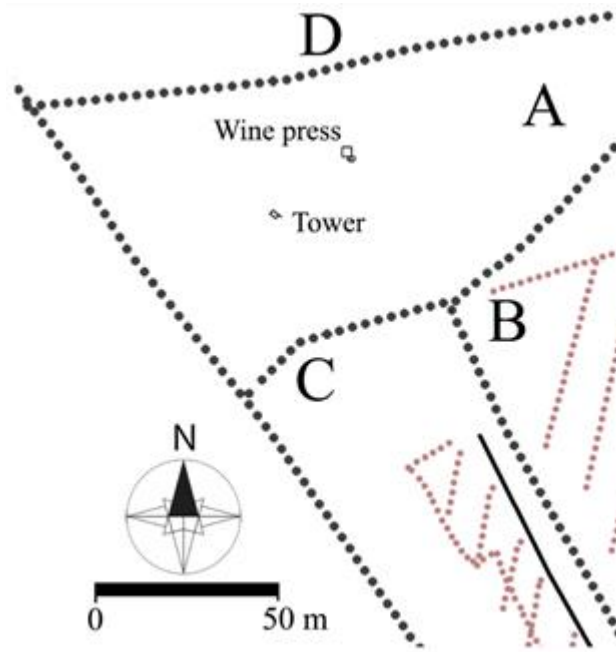


Fig. 11 Sketch plan of Area A with wine press and tower (Nigro *et al.*, 2018).

3.3 Materials Found in the Site

Materials found in the necropolis range from artefacts to human bone remains (Nigro *et al.*, 2018). Both IB/EB IV and MB I-III inhumations were found in primary articulated displacement and they were accompanied by ordinary funerary sets, including pottery vessels, food offerings, personal ornaments and, in some cases, bronze weapons and signet rings with scarabs. The ceramic assemblage shows a wide variety of shapes, from platters to different types of carinated bowls; there are also jugs, juglets and jars, as well as several specialized wares, for example Red Burnished Ware, Tell el-Yahudiyeh Ware, Black or Dark Faced Burnished Ware, the latter basically in the form of small juglets possibly serving as containers of ointments or drugs. In the Middle Bronze Age, tools such as bronze daggers and socketed axes, toggle pins and needles are found to be the regular belongings of male and female individuals, respectively (Nigro *et al.*, 2018).

Chapter 4 Geological Setting

The necropolis of Khalet al-Jam'a is located South-East of Bethlehem (lat. 31.6818666460001; long. 35.2102333120001, Fig. 12), approximately 1.5 Km south of the Church of Nativity (Nigro *et al.*, 2017).

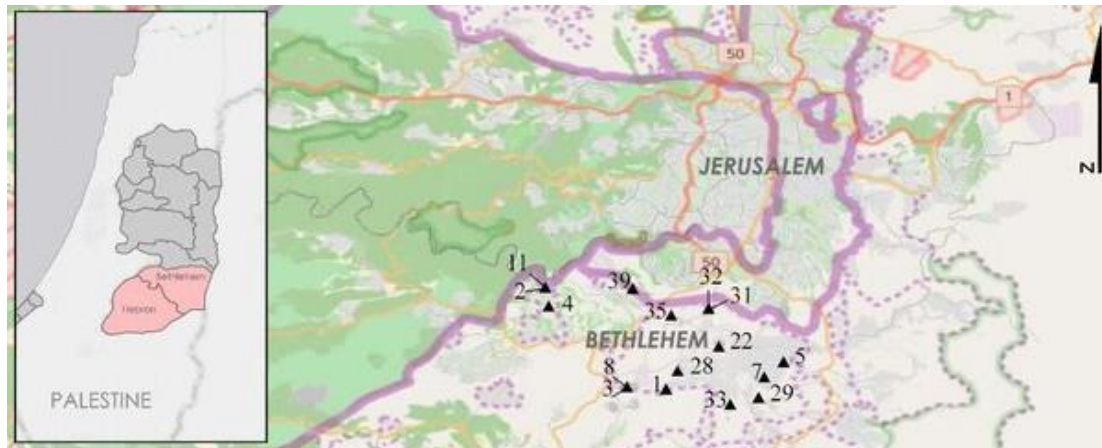


Fig. 12 Comprehensive map of the area of Bethlehem, city and surroundings, and of the archaeological site of interest (n. 33 in the map), developed by Sapienza Expedition-MOTA-DACH, modified after Nigro *et al.*, 2017

The area of Bethlehem is in the southern part of the West Bank (Fig. 13), which is composed of thick sequences of layered limestone, dolomite, chalk and marl (Shalash & Ghanem, 2008; Ghanem *et al.*, 2011).



Fig. 13 Bethlehem in the West Bank, Encyclopedia Britannica (<https://www.britannica.com/place/Bethlehem>)





Specifically, the so-called Bethlehem District, which covers an area of 575 km², is located eight kilometres south of Jerusalem. It borders on the Hebron District to the south and south-west, the Dead Sea to the east and Israel to the west.

This District ranges from the upper Albian stage to the upper Cretaceous series to that of recent formation, as shown in Figure 14 (Applied Research Institute Jerusalem, 1995):

1. Limestones and Marls from the Cenomanian to Turanian ages, as the oldest formations;
2. Chalk and chert formations from the Senonian age;
3. Miocene metamorphic and calcium silicate rocks;
4. Lisan and Samara chinks, marls and conglomerates ranging from Pleistocene to recent ages, as the youngest formations.

Bethlehem District

Legend

-  Chalk, marl, conglomerate
Pleistocene-Holocene
Lisan and Samara formation
-  Metamorphic rocks, mainly calc-silicates
(Miocene) and metamorphism of Senonian
to Neogene rocks
-  Chalk, chert
Senonian
-  Limestone, marl dolomite
Cenomanian-Turonian

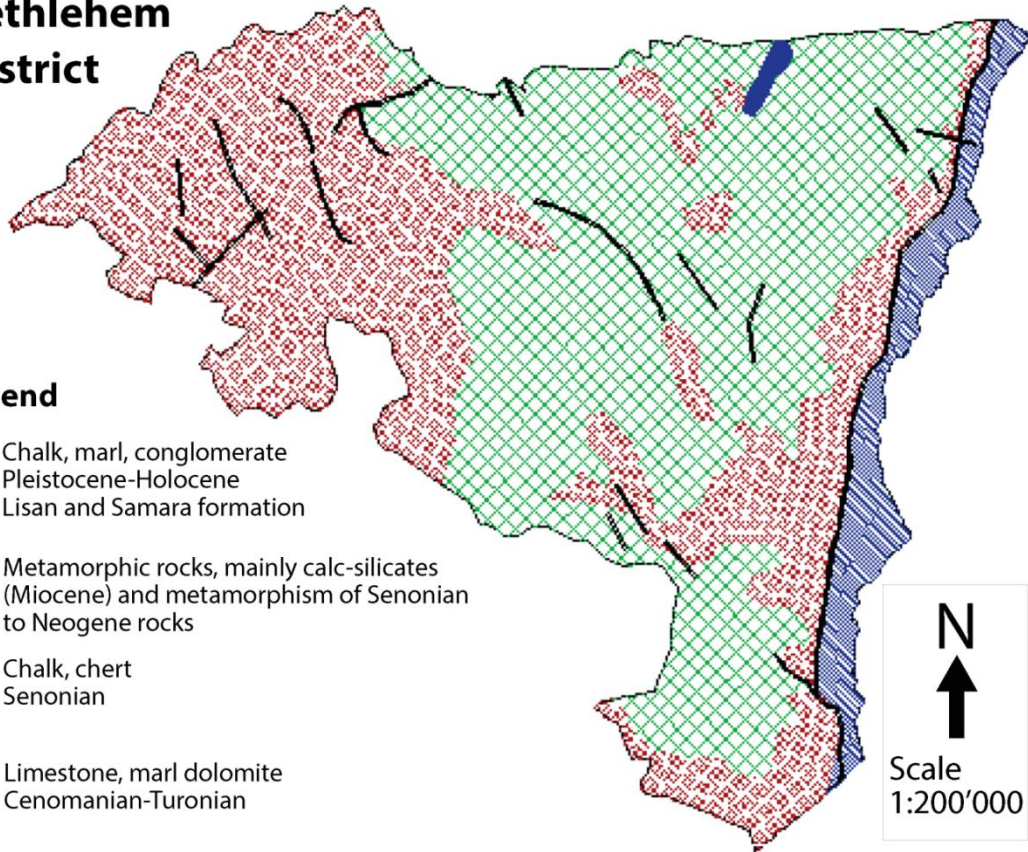


Fig. 14 Geological map of the Bethlehem district, modified after Applied Research Institute Jerusalem, 1995

Chapter 5 Materials and Methods

5.1 Samples

In this study, five ceramic sherds of different wares were selected from Tomb A7 and Tomb C5.

Sample KJ.15.TA7/3

This sample is part of an Iron Age krater and was unearthed from Tomb A7. It probably corresponds to the lip connecting the body part. It is reddish-brown at surface level while the middle layer is grey. The surface is smooth with light luster (Fig. 15).



Fig. 15 Photos of the Sample KJ.15.TA7/3 from both sides (outer, on the left; inner, on the right)

Sample KJ.16.TC5.1/2

This sample is a foot part from a Middle Bronze jug, yielded from Tomb C. The outer surface appears reddish-brown, while the inner part is light brown.



Fig. 16 Photos of the Sample KJ.16.TC5.1/2 from both sides (outer, to the left, inner to the right)

Sample KJ.16.TC5.1/3

This second sample (Fig. 17) from Tomb C is a big piece of a Middle Bronze bowl in khaki colour, which is also the lip part connecting the body. It has a rough surface, with both inner and outer sides having the same colour.



Fig. 17 Photos of the Sample KJ.16.TC5.1/3 from both sides (outer, to the left, inner to the right)

Sample KJ.16.TC5.1/10

This piece of Middle Bronze jar was decorated on its lip with a layered appearance, from the same Tomb C. The surface is rough, in khaki colour and is consistent throughout the whole bulk.



Fig. 18 Photos of the Sample KJ.16.TC5.1/10 from both sides (outer, to the left, inner to the right)

Sample KJ.16.TC5.1/14

This sample is the body piece of a jar dated back to Middle Bronze found in Tomb C. It appears reddish khaki and the surface is rough but consistent in both sides.



Fig. 19 Photos of the Sample KJ.16.TC5.1/14 from both sides (outer, to the left, inner to the right)

5.2 Experimental

5.2.1 Optical Microscope

Petrography is the preliminary and essential part for ceramic study, specifically in investigating the mineralogical and textural composition of ceramic artefacts. The utilization of a polarizing light microscope (OM) enables the identification of the different raw materials: minerals, rock fragments and inorganic or organic temper. Furthermore, it could contribute to the study of raw materials provenance and origin, as well as to recognize the different technological procedures followed to make the ceramic items (from shaping to firing), thus providing clues on the function of the ceramic. Moreover, the information could be used to reconstruct the story hidden behind, such as trades or exchanges of raw materials and ceramics, and further reconstruct the past society.

Each sherd is cut perpendicularly to the surface and polished on one side, and later glued on a glass slide by thermosetting epoxy resin. The sample is then ground down to a thickness of 20 μm . At this thickness level different minerals display the interference colours under polarizing microscope, which will serve as identification of mineral themselves. These thin sections were examined under the polarizing microscopy according to Whitbread (1986, 1995) criteria with the aim to identify their microstructure and textural features. These features are the abundance, shape, roundness, spacing and the alignment of inclusions; the amount, shape, size and alignment of voids; as well as the nature of the matrix, such as the abundance, the colour, homogeneity, optical activity and whether the matrix is calcareous or not.

Samples were analysed by a Zeiss D-7082 Oberkochen microscope at the Department of Earth Sciences of Sapienza University of Rome, at both plane polarize light (PPL) and crossed polarized light (XP).

5.2.2 X-ray Diffraction

X-ray powder diffraction (XRD) is used for studying the mineralogical composition of ceramics. The minerals own the characteristic of crystalline structure, where atoms are periodically arranged in three-dimensions and the planes within are characterized by specific d-space values. Being the wavelength of X-rays at same magnitude scale of the crystal spacing, it allows X-rays to be diffracted and this yields characteristic diffraction patterns for each mineral species. Thus, it may allow the identification of

the main minerals in the ceramic, their quantity and the structural changes they have undergone. Interpreting the diffraction patterns provides information on features and properties of the ceramics, together with other technological aspects such as their provenance and firing temperature.

The samples were peeled into small pieces, grinded to powder and placed on a sample holder for the analysis. The collected data were given as diffraction patterns, where the diffracted intensity, I , is a function of the scattering angle, 2θ .

XRD analyses were performed using a Siemens D5000 automatic powder diffractometer at the Department of Earth Sciences of Sapienza University of Rome.

5.2.3 Scanning electron microscope

Another useful technique in the analysis of archaeological ceramics is Scanning Electron Microscopy coupled with Energy Dispersive Spectrometry (SEM-EDS) to study the chemical composition, the abundance and even the distribution of inclusions. Two kinds of interactions electron beam-material may be analysed: backscattered electrons (BSE) giving information on chemical differences, as the BSE image permits to characterize the distribution of elements based on their atomic number, where a "brighter" BSE intensity correlates with greater average Z in the sample, and "dark" areas have lower average Z ; secondary electrons (SE) give images, on the other hand, that represent the morphology of the sample. In this study we also applied the elemental mapping of a few areas in order to analyse the distribution and abundance of interested elements in 2-dimensions images.

Four of five thin sections (the only exception being KJ.16.TC5.1/2) were carbon-coated and analysed with a FEI-Quanta 400 instrument, operating at 20 kV, equipped with an energy dispersive X-ray analysis detector (Department of Earth Sciences, Sapienza University, Rome, Italy).

Chapter 6 Results

6.1 Petrographic analysis

Petrographic analysis was carried out first, to gain a preliminary inspection of all the samples, in the attempt to acquire details on the microstructure, specifically the features of inclusions, voids and matrix.

KJ.15.TA7/3

Sample KJ.15.TA7/3 (Fig. 20) displays a unimodal grain size distribution of the inclusions, which are estimated around 30%. They are equant and elongated, from angular to sub-rounded and from open to single-spaced, with no alignment. The inclusions are mainly characterized by calcareous rocks, with the presence of fine quartz and sedimentary siliceous rocks. Some iron oxide nodules have also been identified in the calcareous matrix. The matrix is optically active, brownish-green and brownish-red in colour (in PPL) but not homogeneous. The pores are poor (3%), mainly consisting of micro-vesicles, macro- and meso-*vughs* aligned to the margin of the sample. The presence of micro-fossils is also captured and displayed in Fig. 20.

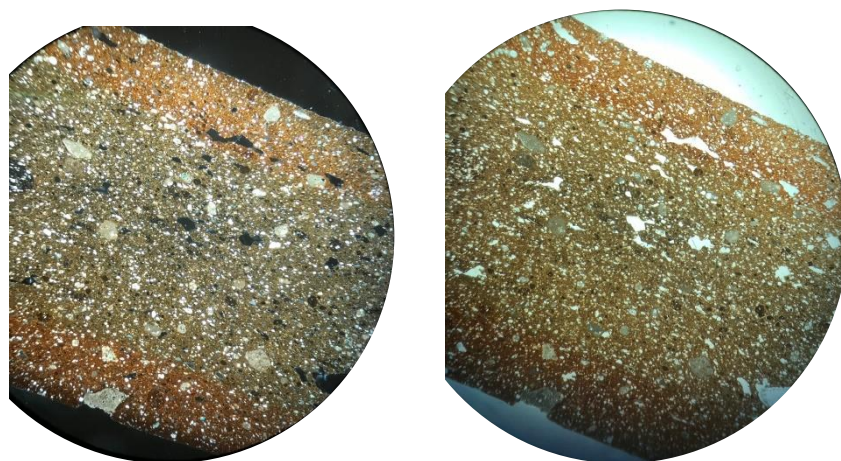


Fig. 20 optical microscope image of sample KJ.15.TA7/3 (mag 2.5x) at crossed polarized light (left) and at plane polarize light (right).

KJ.16.TC5.1/2

Sample KJ.16.TC5.1/2 (Fig. 21) displayed equant and elongated inclusions (30%) distributed from double to open-spaced, from sub-angular to sub-rounded in a reddish-brown calcareous matrix, optically active. The inclusions are mainly represented by predominant fine quartz (equant and elongated, sub-angular, 0.1-0.6

mm), together with diffuse fragments of sedimentary calcareous rocks (equant and elongated, sub-angular, 0.1-0.6 mm), fine, rare calcite crystals (equant and elongated, sub-angular, 0.1-0.6 mm) and fragments of fossils (equant and elongated, sub-angular, 0.1-0.6 mm) .The inclusions present a unimodal grain size distribution. The scarce porosity (3%) is composed of macro- to micro-*vughs* and from meso- to micro-vesicles, aligned to the margin of the sample.

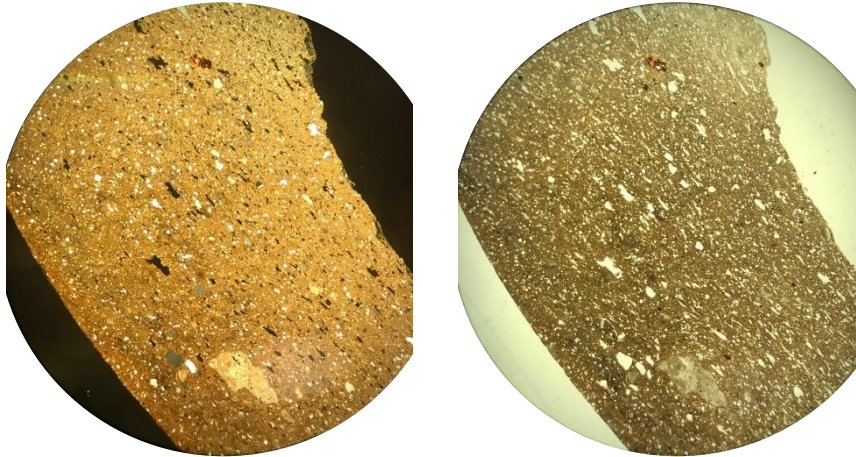


Fig. 21 optical microscope image of sample KJ.16.TC5.1/2 (mag 2.5x) at crossed polarized light (left) and at plane polarize light (right).

KJ.16.TC5/1/3

In sample KJ.16.TC5/1/3 only equant inclusions (40%) are observed, from angular to sub-rounded, from single to open-spaced with a unimodal grain size distribution. The predominant mineral is fine quartz, with the presence of calcareous inclusions, fragments of sedimentary calcareous rocks and fine dolomite, which showed altered margins. The homogeneous calcareous matrix is brown in colour, having no optical activity. The voids are the most abundant among all the five samples and are estimated about 5-10%. They are mainly *vughs*, ranging from macro- to micro-, while only micro-sized vesicles are observed. All the voids are aligned to the margins of the sample.

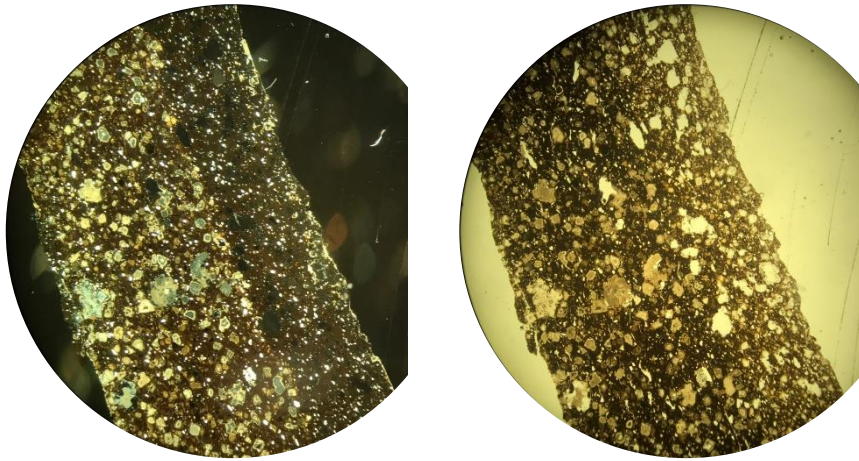


Fig. 22 optical microscope image of sample KJ.16.TC5.1/3 (mag 2.5x) at crossed polarized light (left) and at plane polarize light (right).

KJ.16.TC5.1/10

The reddish-brown matrix of sample KJ.16.TC5.1/10 is calcareous, optically active and homogeneous. The equant and elongated inclusions, from angular to sub-rounded, with closed-single spacing, are distributed in a unimodal way. This sample has the most abundant inclusions, up to 50%. It was possible to identify predominant fragments of sedimentary calcareous rocks, rare quartz and fossils, and some altered dolomite.

The low porosity (3%) consists of meso- and micro-vesicles, together with the presence of *vughs* from macro- to micro-, all aligned to the margins of the sample.

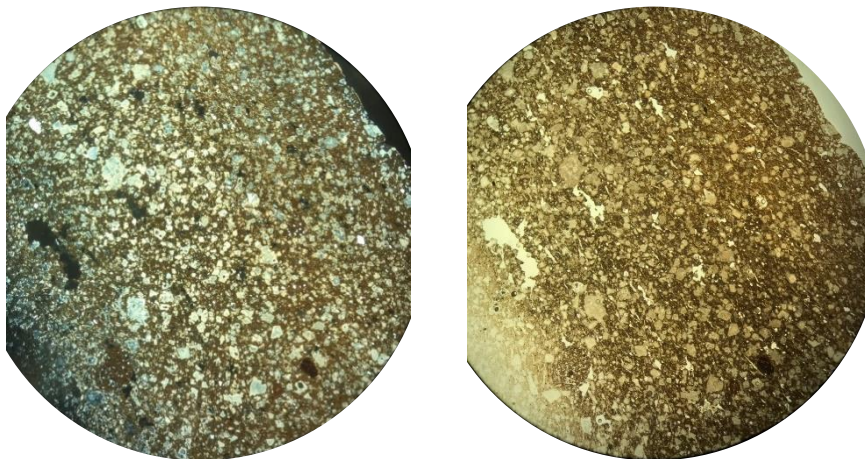


Fig. 23 optical microscope image of sample KJ.16.TC5.1/10 (mag 2.5x) at crossed polarized light (left) and at plane polarize light (right).

KJ.16.TC5.1/14

Sample KJ.16.TC5.1/14 shows quite different petrographic features: it is characterized by predominant calcite and dolomite crystals. Quartz appears less abundant here. Fragments of sedimentary calcareous rocks and some fragments of siliceous rocks are diffuse. Rare iron oxide nodules are also identified. This sample is homogeneous, the inclusions appear equant and elongated (30%), unimodally distributed, from open to single spaced, with a shape ranging from angular to sub-rounded.

The calcareous matrix is brownish-green in PPL and optically active. Pores (5%) consist mainly of meso- and micro-vesicles with some larger *vughs* (from mega- to meso-) aligned to the margin of the sample.

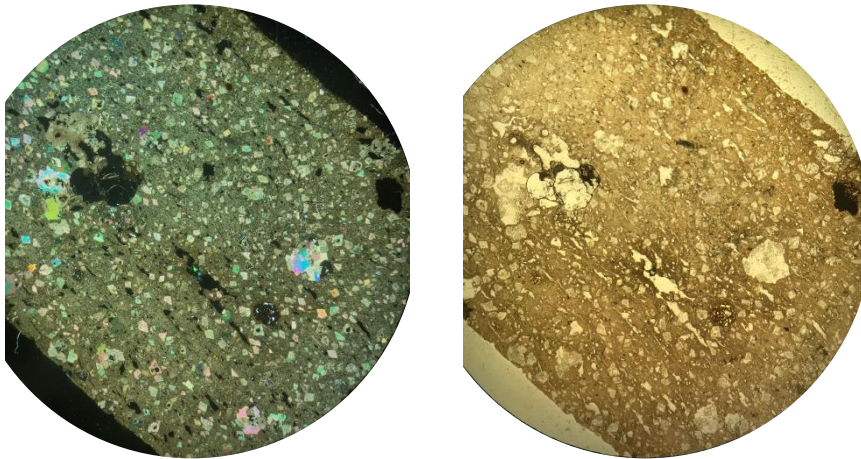


Fig. 24 optical microscope image of sample KJ.16.TC5.1/14 (mag 2.5x) at crossed polarized light(left) and at plane polarize light(right).

Table 1: Summary of the main microscopic features of the samples under OM observation

| Sample | Pores | Matrix | Inclusions | |
|---------------|------------------------|----------------------|--|---|
| KJ.15.TA7/3 | 3% | 67% | 30% | <u>predominant</u> : calcareous rocks, equant-elongated, |
| | micro vesicles | non-homogeneous | equant-elongated, from angular | angular to sub-rounded |
| | macro- meso-vughs | calcareous | to sub-rounded, open to single | <u>present</u> : fine quartz, sedimentary siliceous rocks, equant-elongated, angular to sub-rounded |
| | | optical activity | spaced, not aligned to margins, unimodal grain size distribution | <u>rare</u> : iron oxide nodules, equant, sub-rounded to rounded; microfossils |
| KJ.16.TC5.1/2 | 3% | 67% | 30% | <u>predominant</u> : fine quartz, equant-elongated, sub-angular, 0.1-0.6mm |
| | meso-micro vesicles | homogeneous | equant-elongated, from sub- | <u>present</u> : sedimentary calcareous rocks, equant-elongated, sub-angular, 0.1-0.6mm |
| | macro-meso-micro vughs | calcareous | angular to sub-rounded, double | <u>rare</u> : fine calcite crystals, equant-elongated, sub-angular, 0.1-0.6mm; fragments of fossils |
| | | optical activity | to open spaced, not aligned to margins, unimodal grain size distribution | |
| KJ.16.TC5/1/3 | 5-10% | 40-45% | 40% | <u>predominant</u> : fine quartz, equant, sub-angular |
| | micro vesicles | homogeneous | equant, from angular to sub- | <u>present</u> : calcareous inclusions, sedimentary calcareous rocks, fine dolomite |
| | macro-meso-micro vughs | calcareous | rounded, single to open | |
| | | non-optical activity | spaced, not aligned to margins, unimodal grain size distribution | |

(continue to next page)

| Sample | Pores | Matrix | Inclusions | |
|----------------|------------------------|------------------|---|---|
| KJ.16.TC5/1/10 | 3% | 47% | 50% | <u>predominant:</u> fragment of sedimentary calcareous rocks, |
| | meso-micro vesicles | homogeneous | equant-elongated, from angular | equant, angular to sub-angular |
| | macro-meso-micro vughs | calcareous | to sub-rounded, closed to single | <u>present:</u> altered dolomite |
| | | optical activity | spaced, not aligned to margins, unimodal grain size distribution | <u>rare:</u> quartz, micro-fossils |
| KJ.16.TC5/1/14 | 5% | 65% | 30% | <u>predominant:</u> calcite and dolomite crystals, |
| | equant-elongated, | homogeneous | equant-elongated, from angular | angular to sub-rounded |
| | meso-micro vesicles | calcareous | to sub-rounded, open to single | <u>present:</u> quartz, sedimentary calcareous rocks, siliceous |
| | mega-meso vughs | optical activity | spaced, not aligned to margins, unimodal grain size distribution | rocks <u>rare:</u> iron oxide nodules, equant, sub-rounded |

6.2 X-ray diffraction analysis

KJ.15.TA7/3

This sample is mainly composed by quartz, together with minor calcite and K-feldspar. Plagioclase and clay minerals are also present.

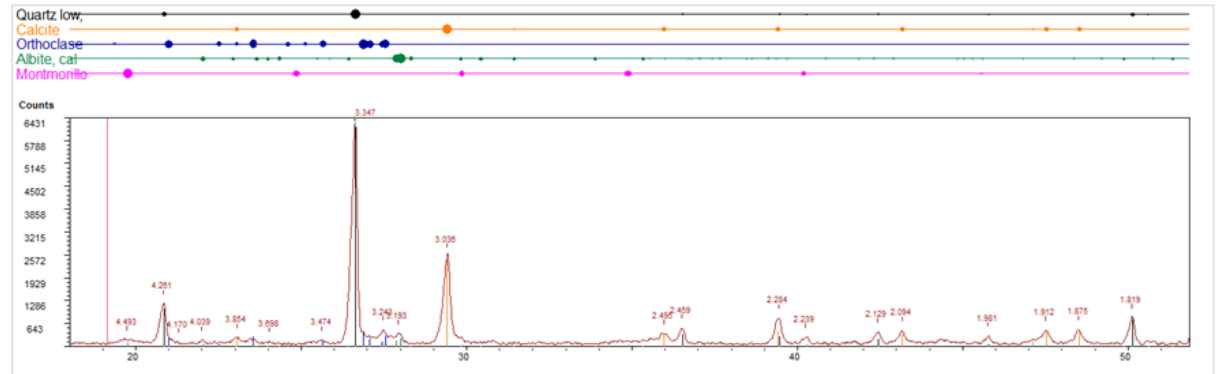


Fig. 25 Diffraction pattern of sample KJ.15.TA7/3

KJ.16.TC5.1/2

In this jug the most abundant mineral is calcite, followed by a minor percentage of quartz. Clay minerals are also present. There are traces of K-feldspar, plagioclase, dolomite and olivine.

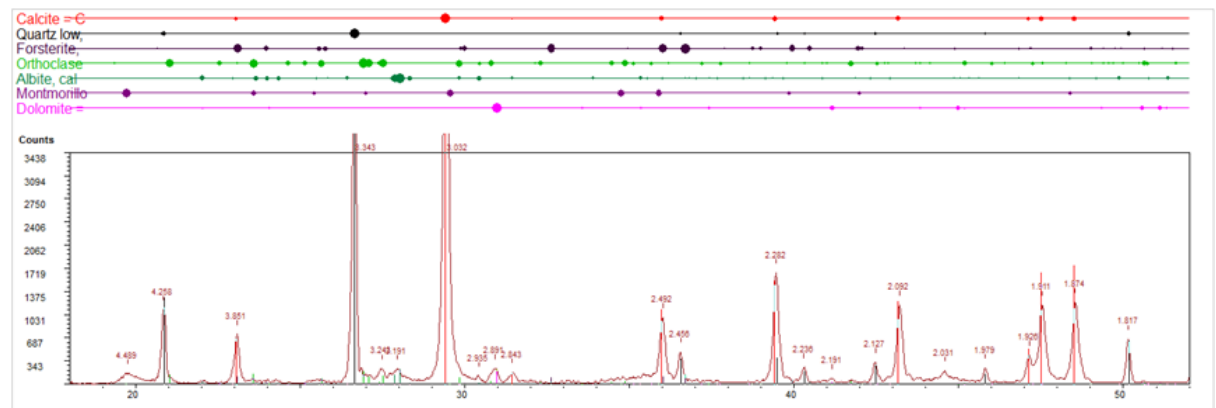


Fig. 26 Diffraction pattern of sample KJ.16.TC5.1/2

KJ.16.TC5/1/3

This bowl sherd is characterized by the presence of quartz, plagioclase, diopside and scarce calcite, K-feldspar and wollastonite. Gehlenite appears in trace amount.

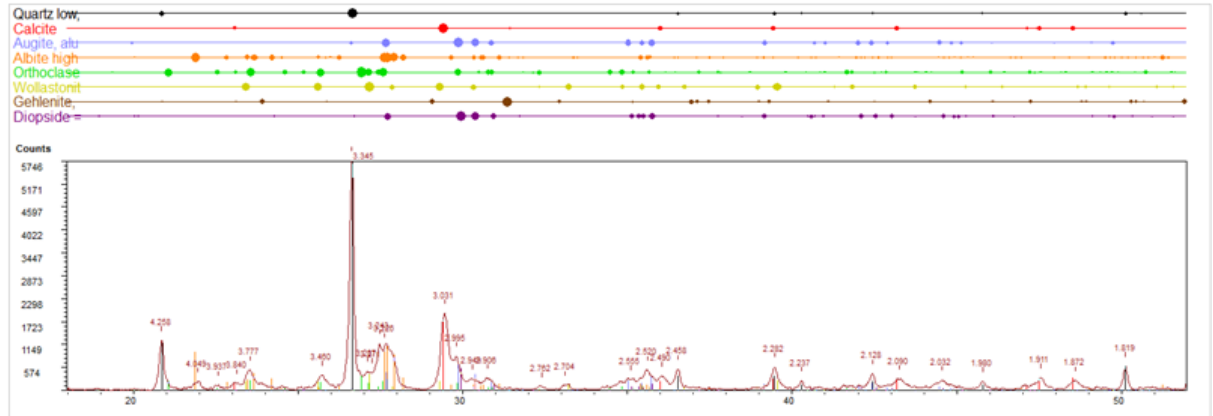


Fig. 27 Diffraction pattern of sample KJ.16.TC5.1/3

KJ.16.TC5.1/10

This sample is mainly composed of quartz, K-feldspar, plagioclase, diopside and orthopyroxene. Calcite is less abundant. Small quantities of olivine and aragonite were detected. Wollastonite also appeared in fair amount in this sample.

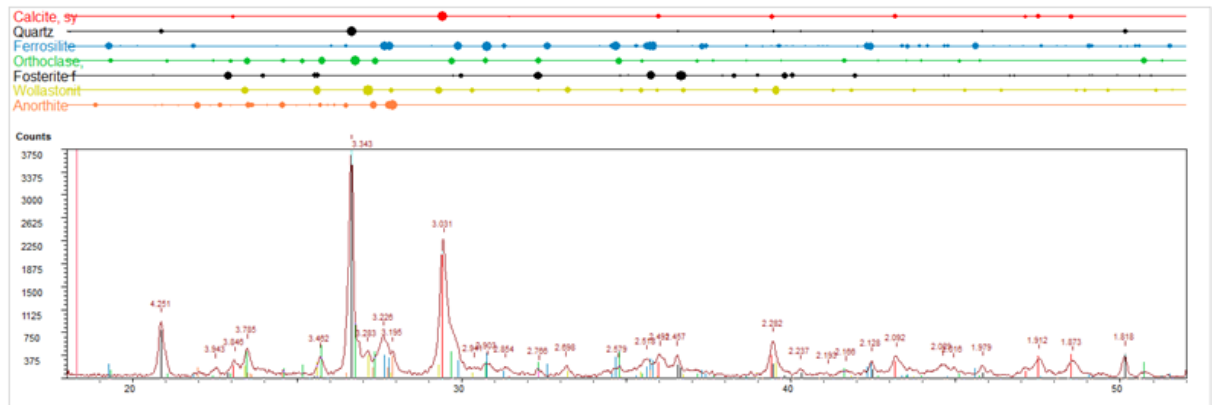


Fig. 28 Diffraction pattern of sample KJ.16.TC5.1/10

KJ.16.TC5.1/14

Calcite predominates in the mineral composition of this jar sherd. Clay minerals and dolomite are less abundant.

Scarce quartz and K-feldspar coexist with trace-amount olivine.

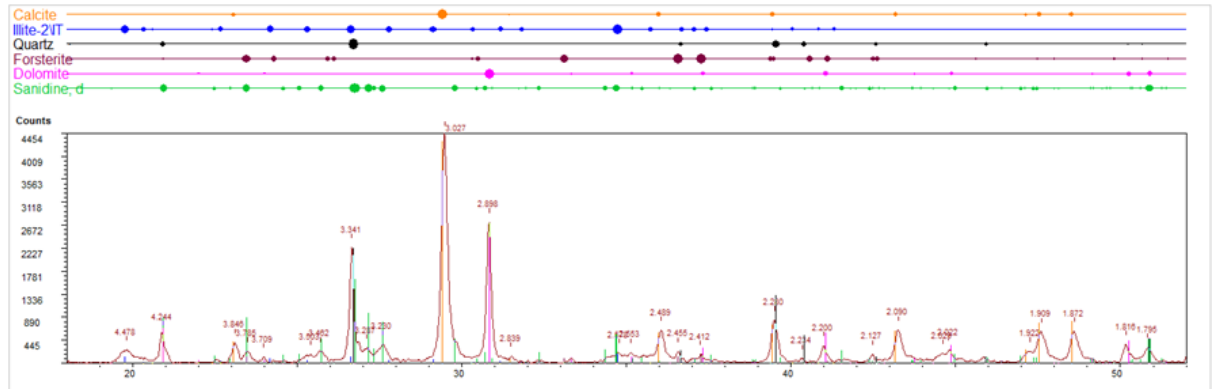


Fig. 29 Diffraction pattern of sample KJ.16.TC5.1/14

Table 2: XRD results of analyzed ceramic samples. Qtz: quartz, Cal: calcite, Kfs: K-feldspar, Pl: Plagioclase, Ill-Mnt: Illite- Montmorillonite, Hem: Hematite, Di: Diopside, Gh: Gehlenite, Dol: Dolomite, Opx: Orthopyroxene, Ol: Olivine, Arg: Aragonite, Wo: Wollastonite; ++++ very abundant 70-50%; +++ abundant 50-30%; ++ present 30-15%; + scarce 15-5%; tr. Traces <5%)

| Sample | Qtz | Cal | Kfs | Pl | Ill-Mnt | Di | Gh | Dol | Opx | Ol | Arg | Wo |
|----------------|-----|----------|-----|----|---------|----|----|-----|-----|----|-----|----|
| KJ.15.TA7/3 | +++ | ++ | ++ | + | + | | | | | | | |
| KJ.16.TC5.1/2 | ++ | +++ + | tr | tr | + | | | tr | | tr | | |
| KJ.16.TC5.1/3 | ++ | + | + | ++ | | ++ | tr | | | | | + |
| KJ.16.TC5.1/10 | ++ | + | ++ | ++ | | ++ | | | ++ | tr | tr | + |
| KJ.16.TC5.1/14 | + | +++ | + | | ++ | | | ++ | | tr | | |

6.3 Scanning Electron Microscopy coupled with energy dispersive spectroscopy (SEM-EDS)

SEM-EDS analysis was used to define in detail the inclusions as well as give a general chemical composition of the matrix.

KJ.15.TA7/3

The general EDS spectrum of the matrix is shown in Figure 30. The matrix is characterized by high amount of Si, with minor abundance in Al and Ca, minor amount of Fe, K, Mg, Na and Ti.

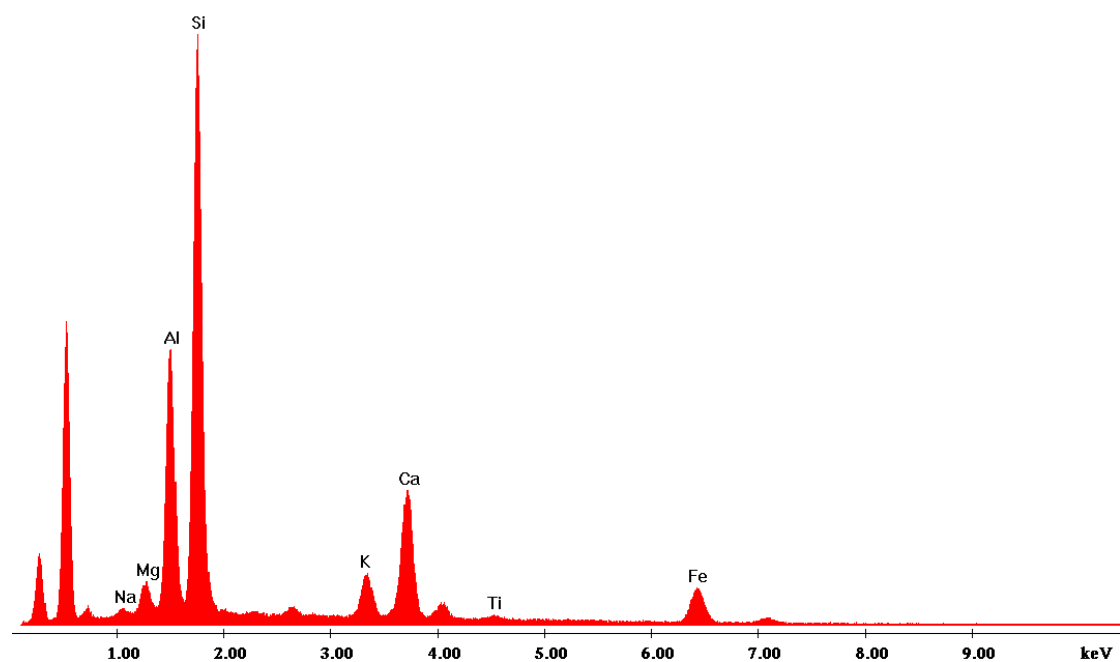


Fig. 30 EDS spectrum of sample KJ.15.TA7/3.

Among the inclusions in KJ.15.TA7/3 sample, SEM-EDS allowed the identification of iron oxide nodules, quartz, fossils and K-feldspar (Fig. 31).

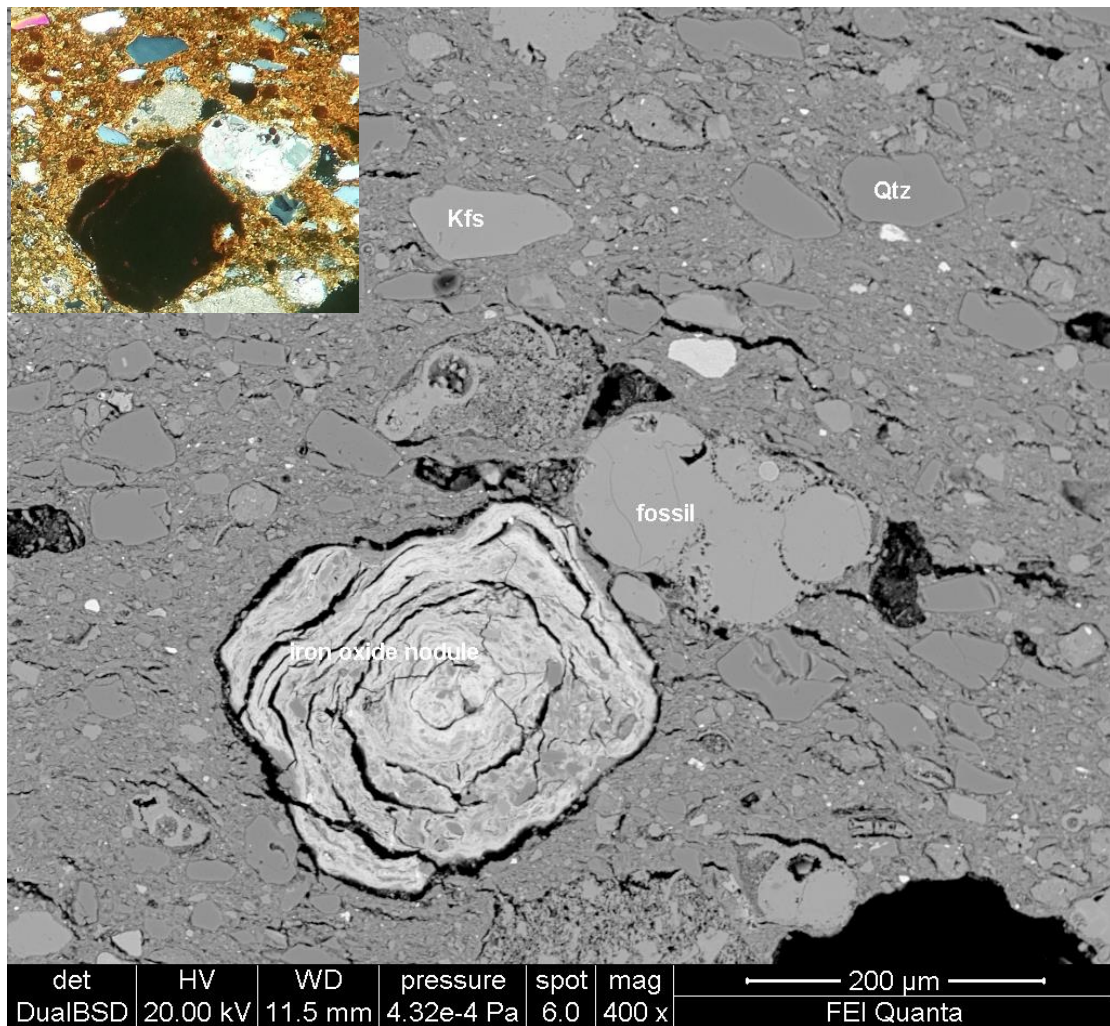


Fig. 31 BSE image of sample KJ.15.TA7/3 displaying an iron oxide nodule, some micro-fossils, quartz and k-feldspar, together with the optical microscope image of the same area under XP (top left).

The presence of sedimentary rocks was confirmed by SEM-EDS analysis. It was possible to identify two types of sedimentary rocks: one calcareous, characterized by the presence of fossils (Fig. 32) and the other one siliceous, with crystals of quartz (Fig. 33).

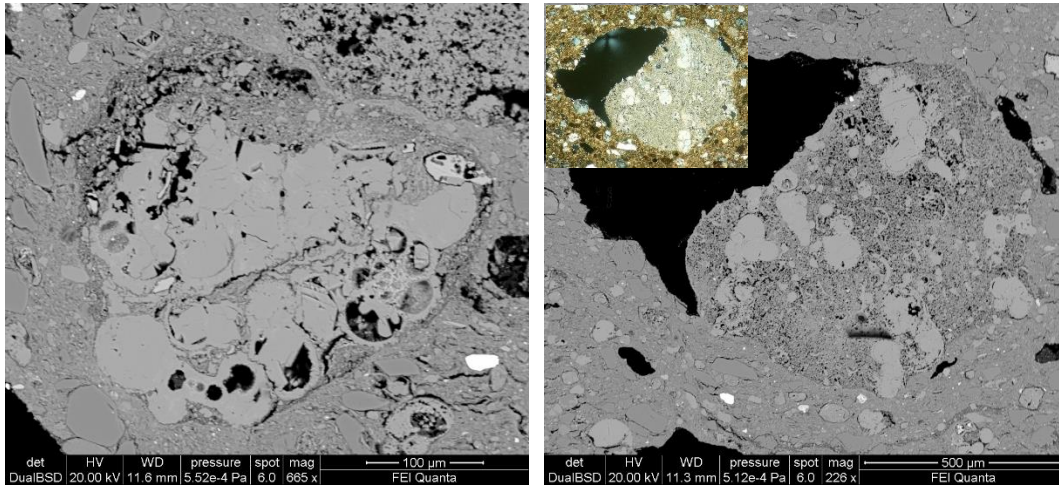


Fig. 32 BSE images of sample KJ.15.TA7/3 displaying sedimentary rock fragments with fossils at different levels of magnification, with the corresponding microscope image of the same fragment under XP placed above.

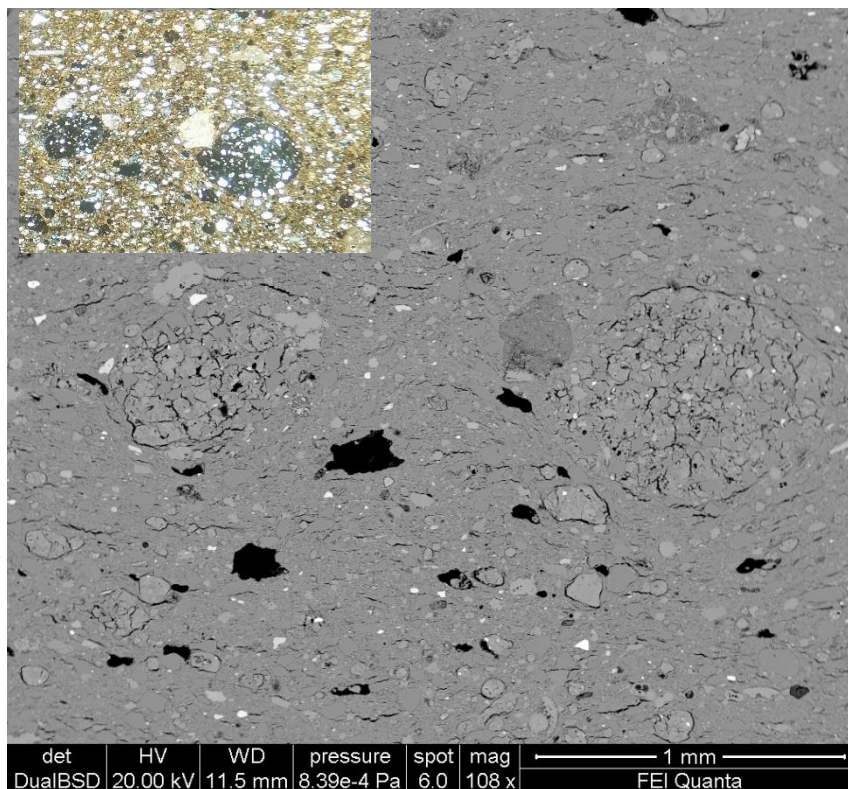


Fig. 33 BSE image of sample KJ.15.TA7/3 displaying sedimentary rock fragments with quartz, and the corresponding OM image of the same area under XP (top left).

In addition, some micro-fossils were identified in the BSE image which are visible in the optical microscope image as well (Fig. 34). These fossils could be distinguished for their particular shape and appearance.

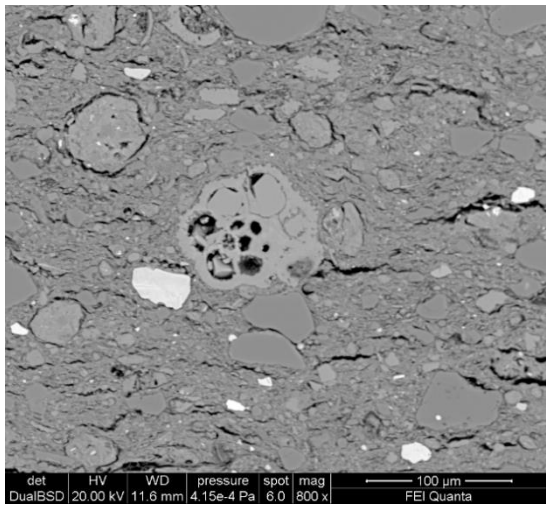
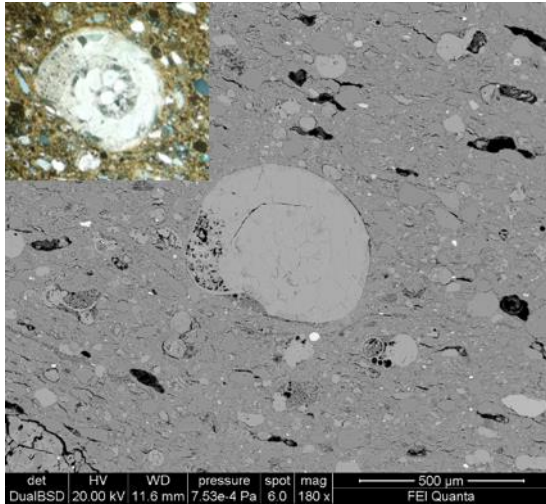


Fig. 34 BSE images of sample KJ.15.TA7/3 showing micro-fossils, with the corresponding OM image of one of them under XP (top left).

Figure 35 shows sedimentary siliceous fragments characterized by quartz crystals (point a) imbedded into the matrix (point b) characterized by high amounts of Si. In addition, point b shows a high content of Al, which is identified in the EDS spectrum. There are also iron titanium oxides as shown in the spectrum of point c, which are indicated by the peaks of Ti and Fe.

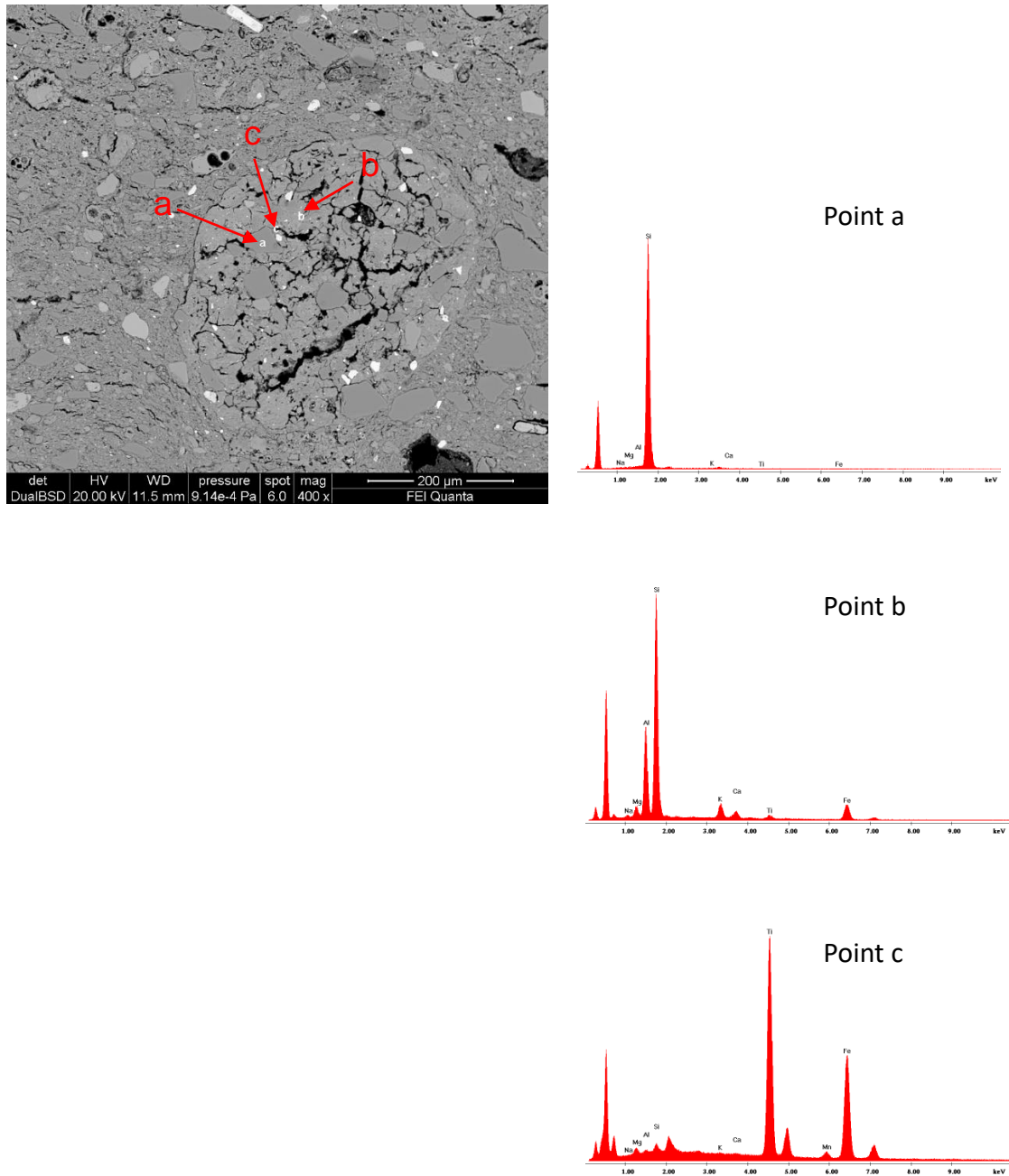
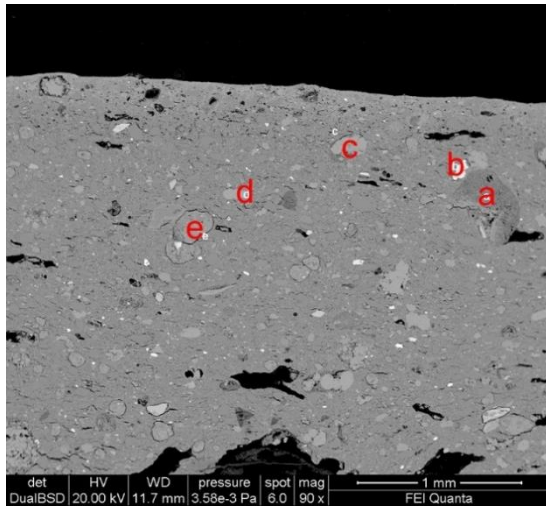
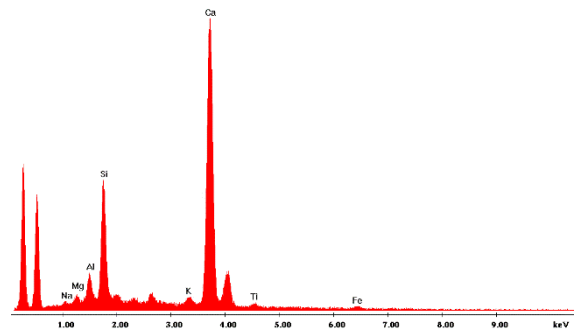


Fig. 35 BSE image of sample KJ.15.TA7/3 displaying a sedimentary rock fragment and the EDS spectra of marked points inside it.

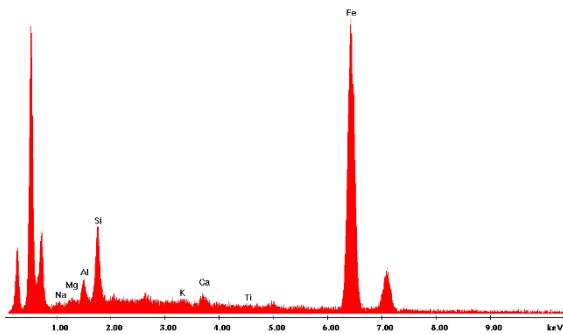
Another image of other inclusions is shown in Figure 36. These inclusions were identified as calcite (point c), iron oxide (point b), and calcareous inclusions at point a and d, while point e has high component of Si and minor Al.



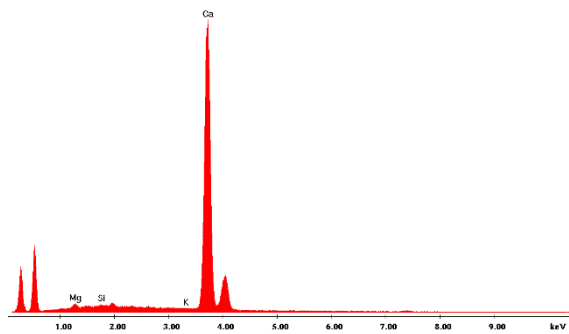
Point a



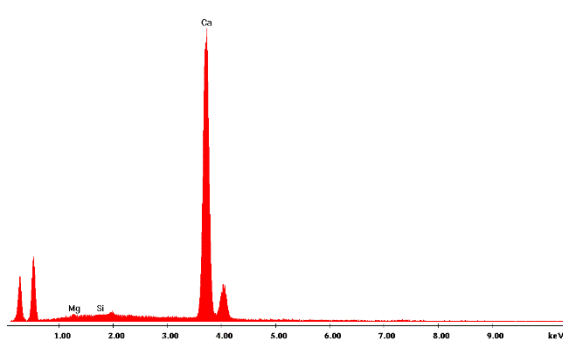
Point b



Point c



Point d



Point e

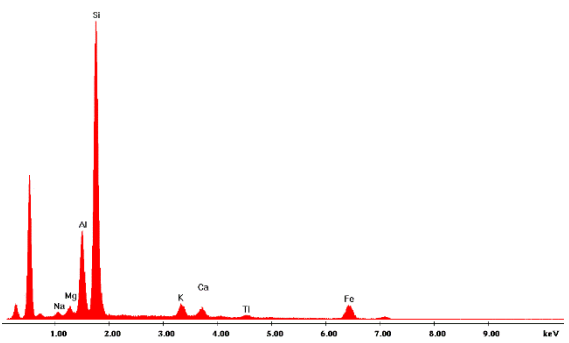


Fig. 36 BSE image of sample KJ.15.TA7/3 displaying the matrix with other inclusions and their corresponding EDS spectra

Moreover, along the surface of the sherd, a distinguishable layer is observed where a secondary layer of calcite is deposited on the vessel (Fig. 37).

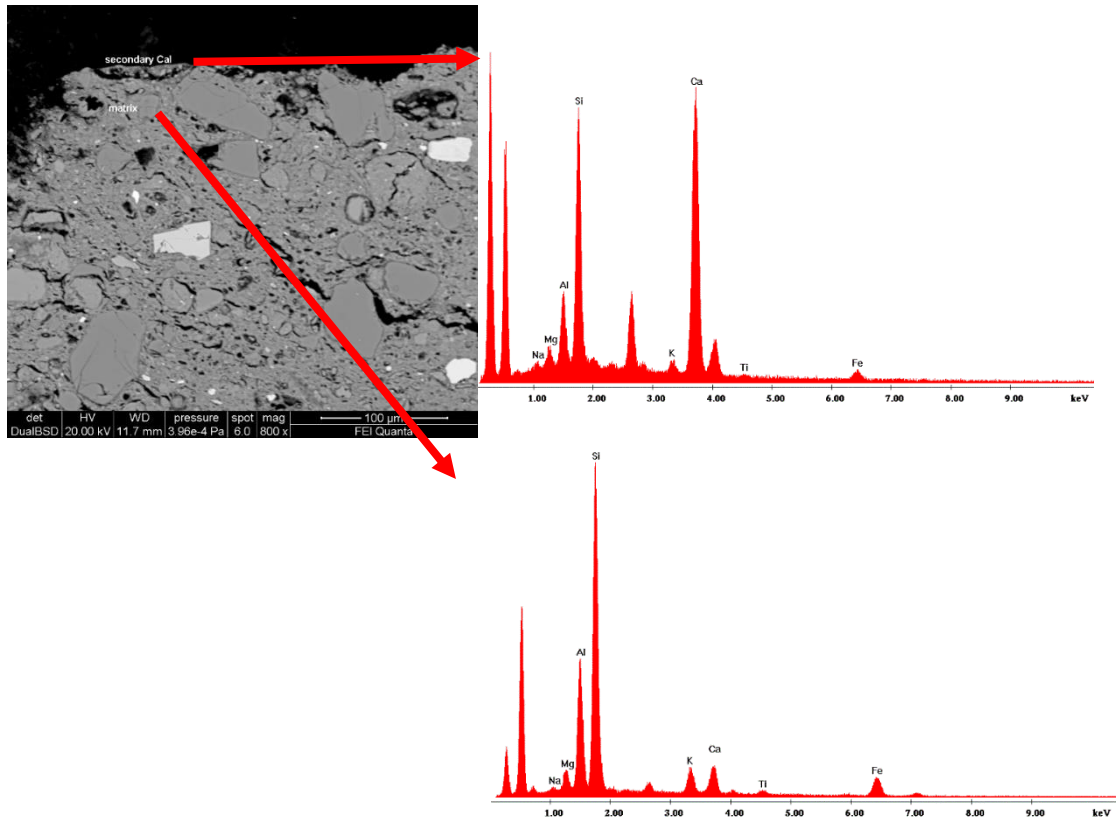


Fig. 37 BSE image of sample KJ.15.TA7/3 displaying the matrix and a recognizable superficial secondary deposit of calcite with the EDS spectra of the matrix (bottom) and of the secondary calcite layer (top).

KJ.16.TC5/1/3

Figure 38 displays the general EDS spectrum of the matrix of sample KJ.16.TC5/1/3, where high Si, minor Al, Ca, and Mg content and K, Na, Ti and Fe in traces were identified.

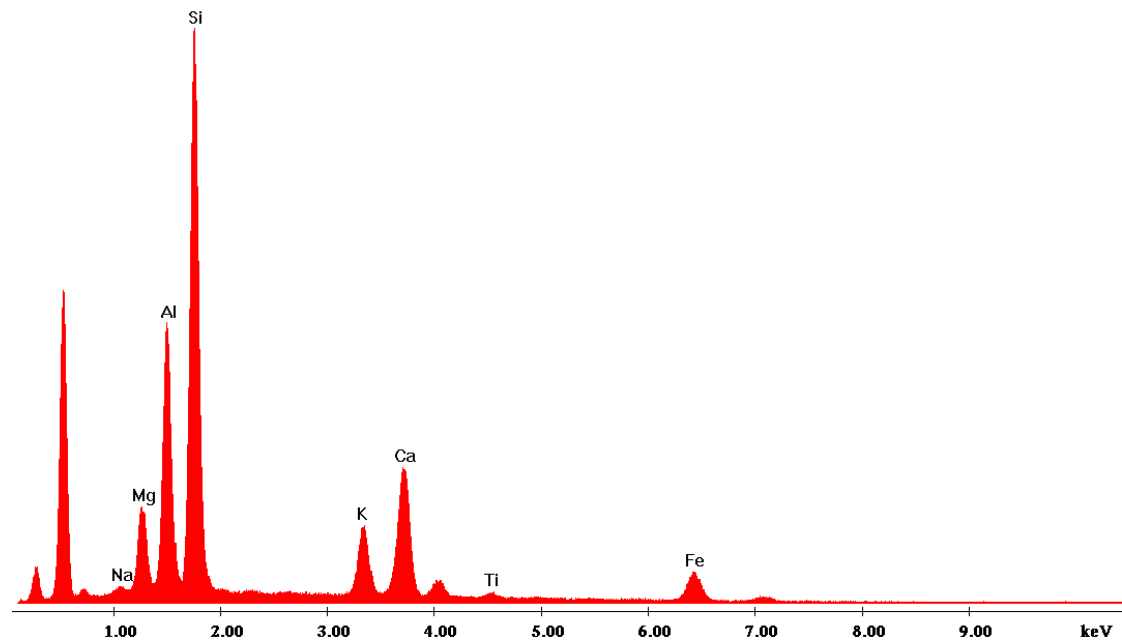
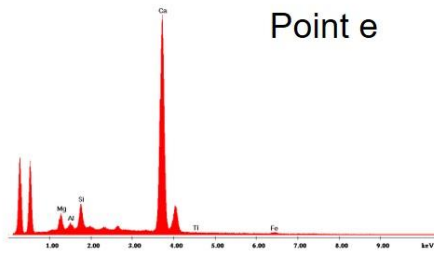
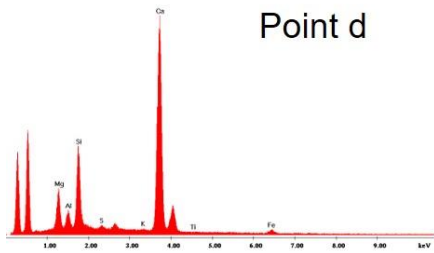
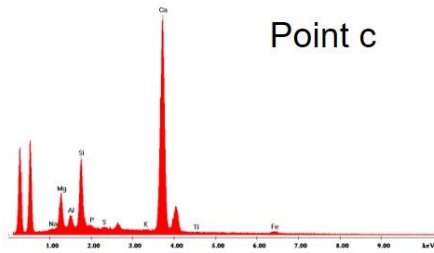
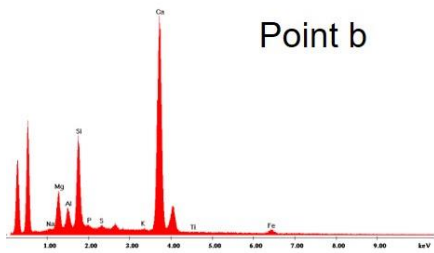
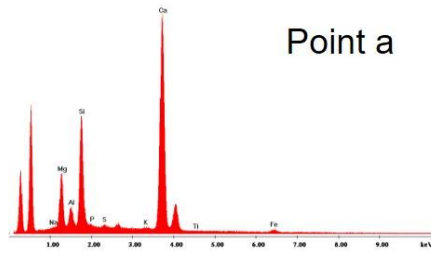
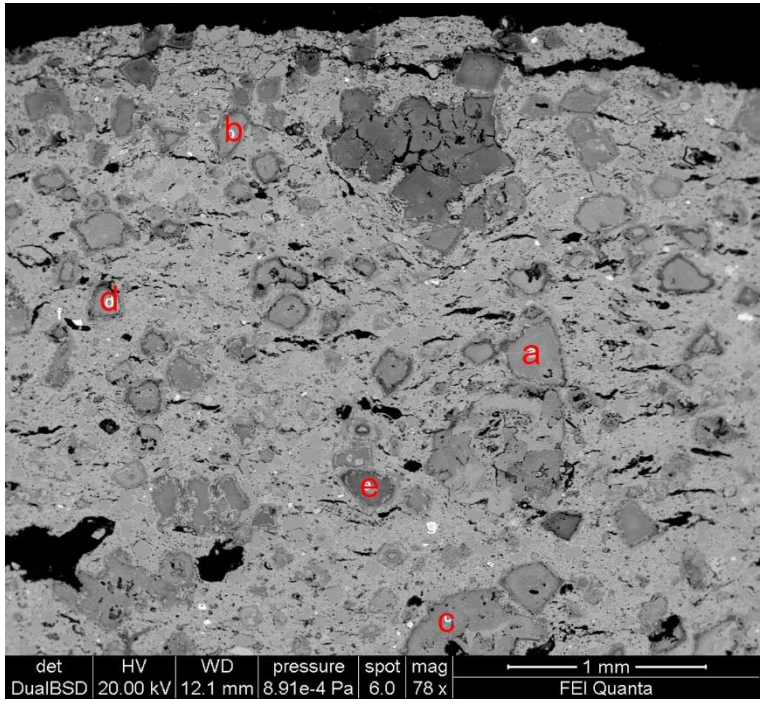


Fig. 38 EDS spectrum of the matrix of sample KJ.16.TC5/1/3

Figure 39 showed the predominant inclusions of the sample and the EDS spectra reveal the presence of calcareous inclusions (point a, b, c, d and e). The presence of ilmenite was confirmed by the peaks of iron and titanium in the spectrum at points f and g.



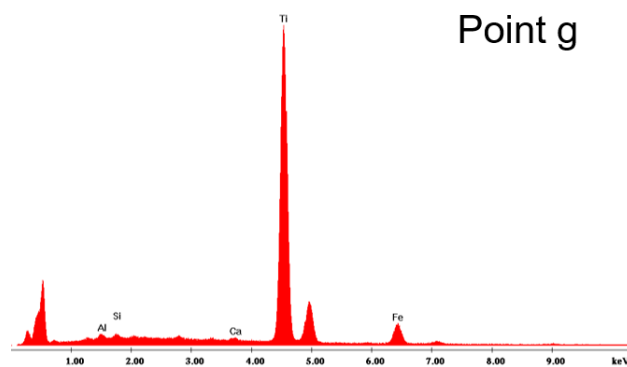
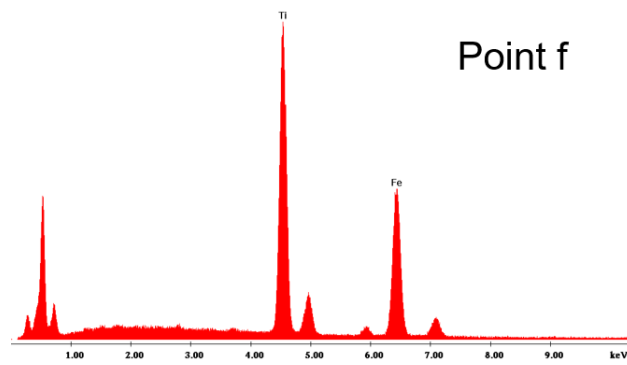
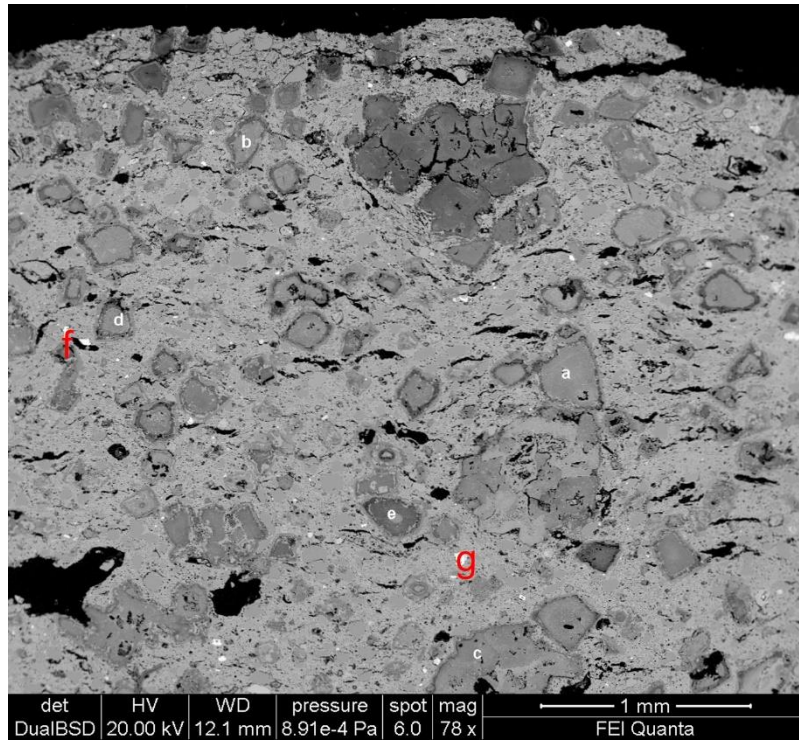


Fig. 39 BSE image of sample KJ.16.TC5/1/3 where several inclusions are recognized and labelled; the corresponding EDS spectra are also shown

An altered inclusion is shown in Figure 40. The composition of 4 points from the 4 distinguishable areas was also investigated in the attempt to figure out the process the sample was undergoing during firing. The spectra collected highlight a different composition from the matrix (point a) to the core (point d). Si content remains high up to the core, where its abundance suddenly decreases. Ca and Al showed the same tendency, with a decreased content in the core. On the contrary, Mg is less abundant in the outer and inner layer, while being higher in the middle layers. The scarce presence of Fe remains constant all along the layers.

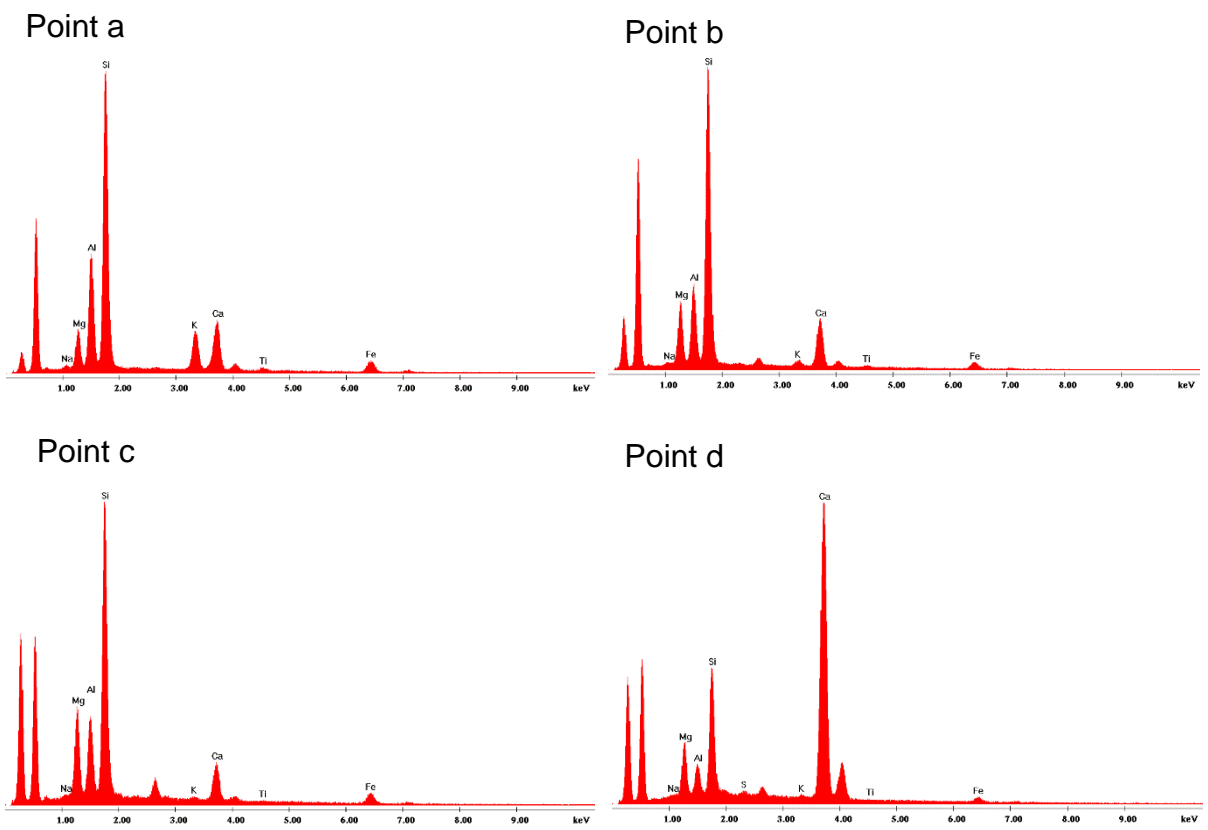
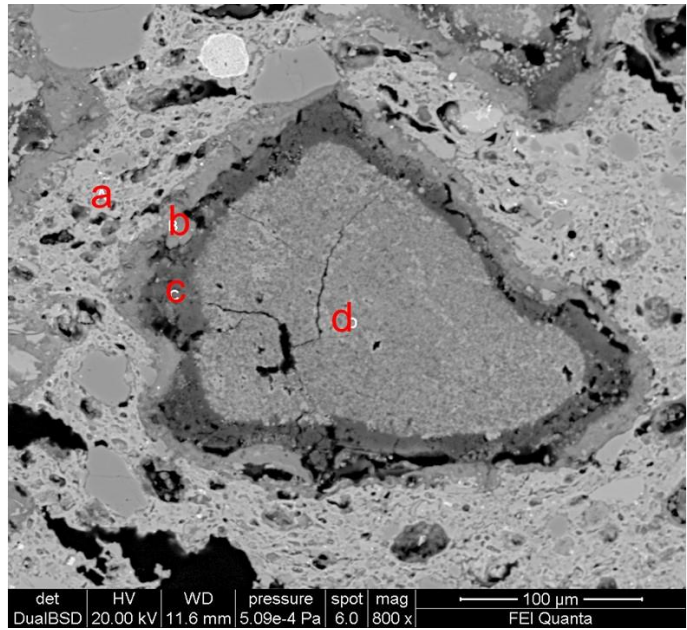
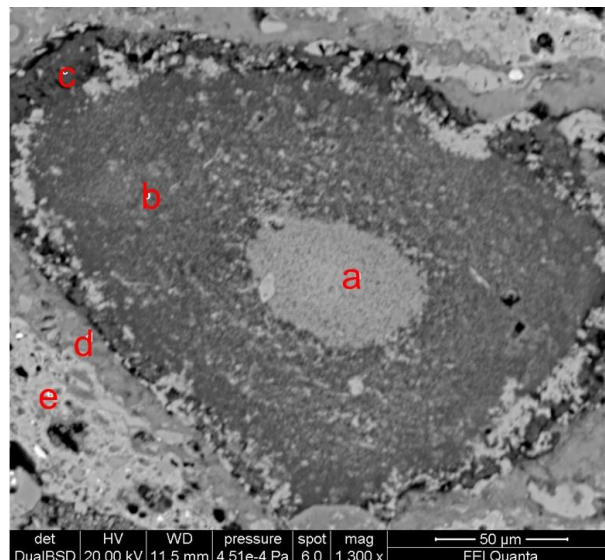


Fig. 40 BSE image of sample KJ.16.TC5/1/3 showing an altered inclusion and the EDS spectra of the layers from the matrix (a) to the altered core (d)

A similar altered inclusion was also found and its progressive change in composition was detected and shown in the spectra below (Fig. 41). Silicon has low content in the core, but while going throughout the core, it becomes higher in abundance and approximately the same amount is found in the outer layer (point c). Calcium generally decreases in the outer parts of the inclusion, but it shows medium abundance at point d. Aluminum content increases while going out of the core. Magnesium shows a fluctuation behaviour in abundance through the alteration. Other elements such as K and Fe, on the other hand, remain in traces.



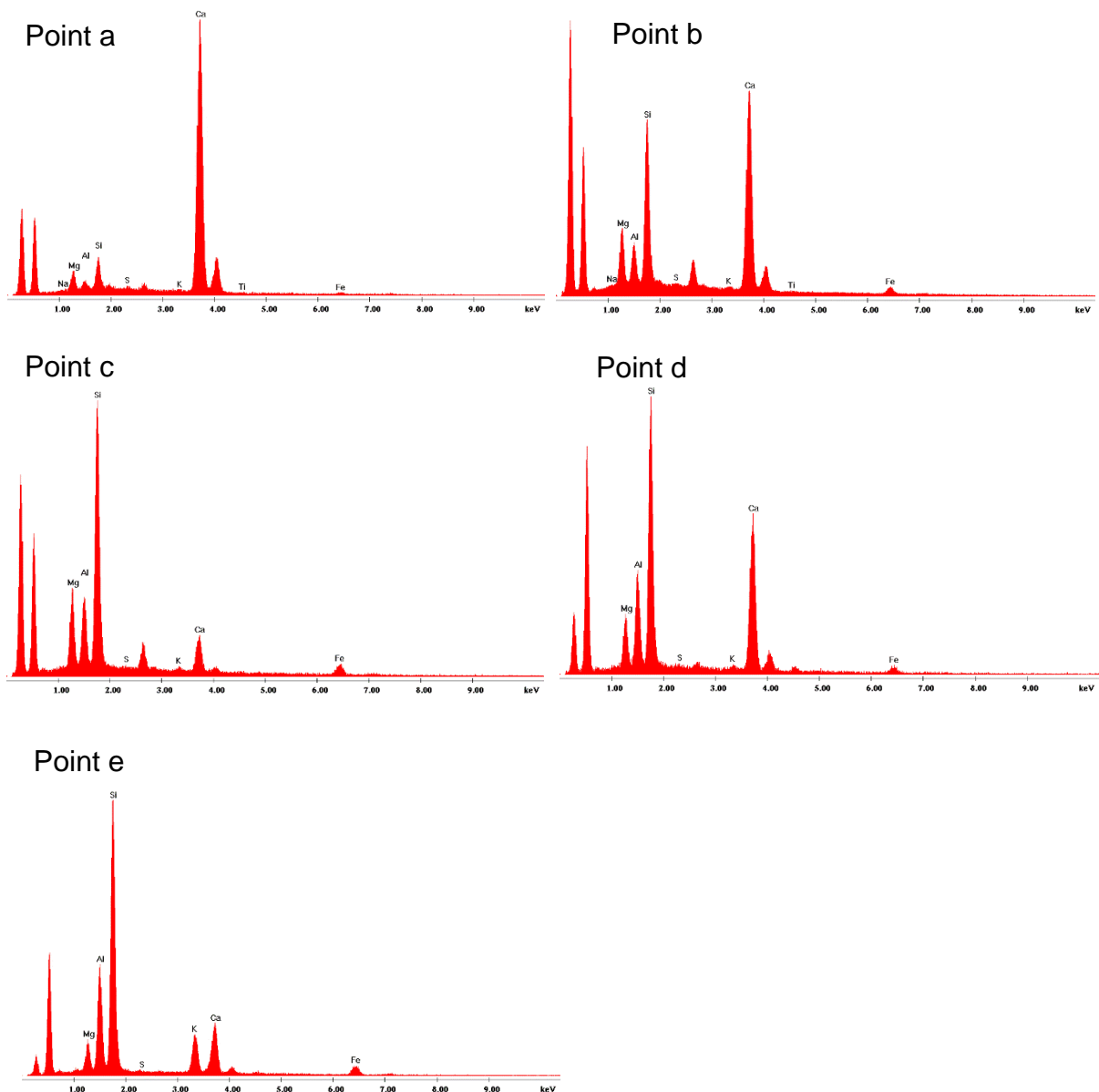


Fig. 41 BSE image of sample KJ.16.TC5/1/3 showing another altered inclusion and the variation in content of some elements from the core (a) to the matrix (e)

Elemental mapping was carried out to analyse in detail the variation in composition of altered inclusions and the EDS maps of specific elements are in Figure 42. The abundance of each element can be seen between the inclusions and margin. Calcium appears more abundant in the inclusions and less in the matrix, while Al, Si and K are more abundant in the matrix and are absent in inclusion particles. Magnesium shows an average distribution in both matrix and inclusions, while Fe, Na can hardly be seen.

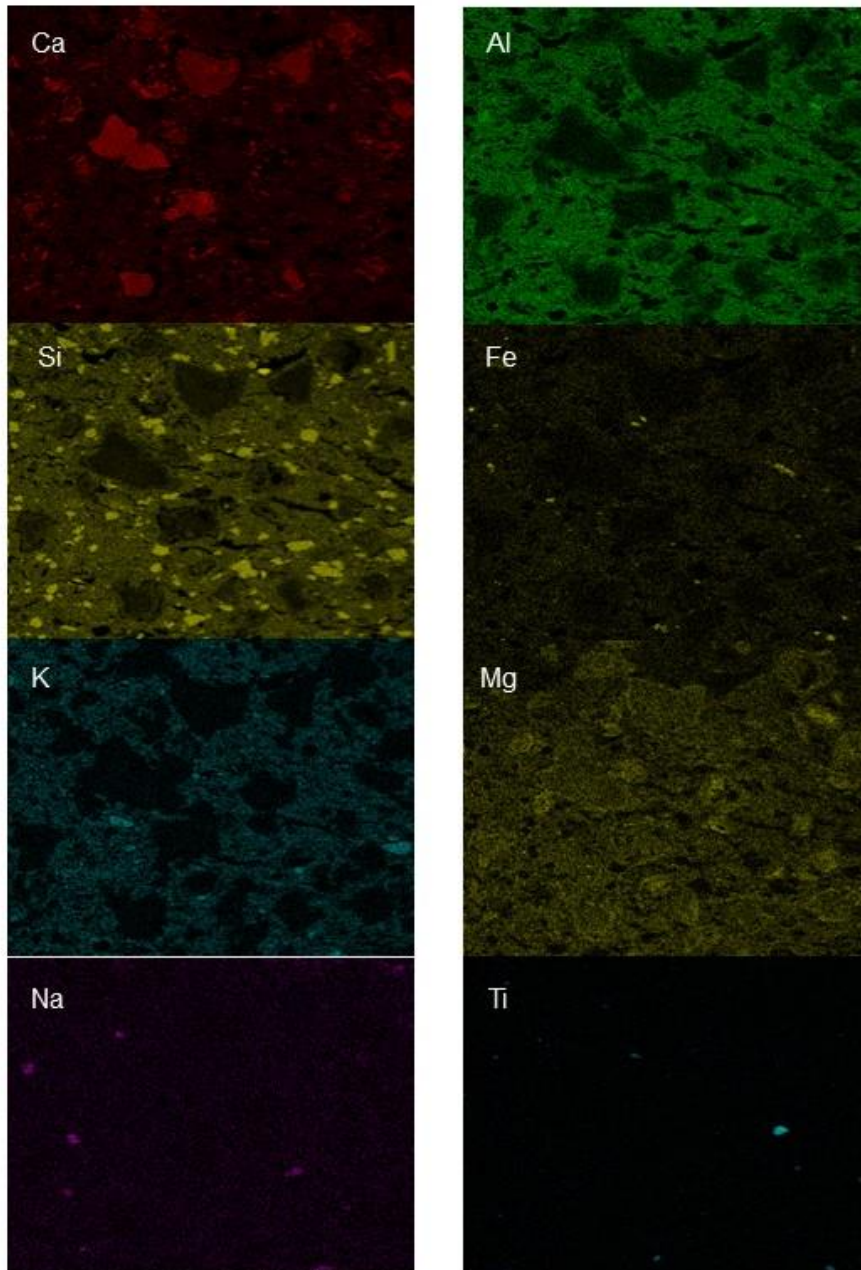
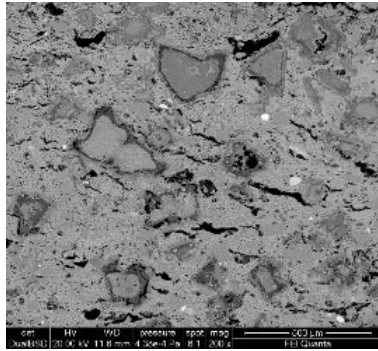


Fig. 42 BSE image of the area and the EDS maps of Ca, Al, Si, Fe, K, Mg, Na, Ti and SE.

KJ.16.TC5.1/10

The general composition of the matrix and some inclusions are shown in Figures 44 and 45. Silicon is the predominant element in the matrix composition, followed by minor Al, less K and rare Mg, K, Ca and Fe.

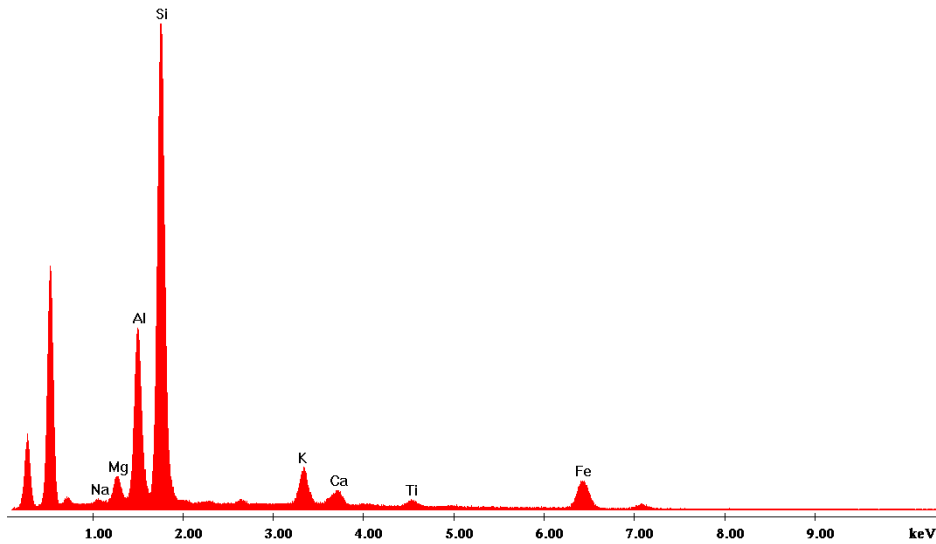
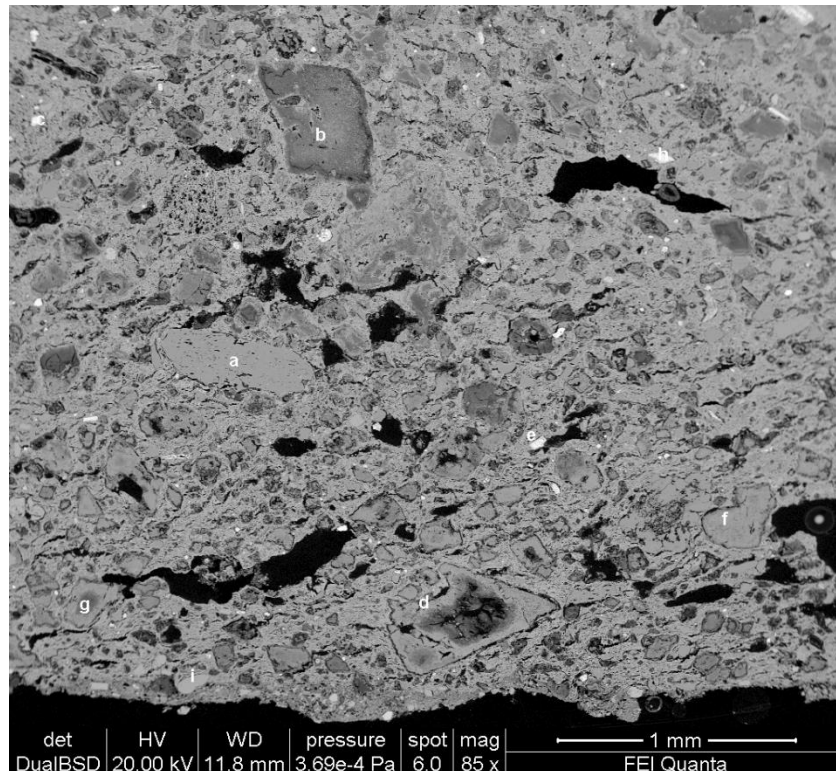
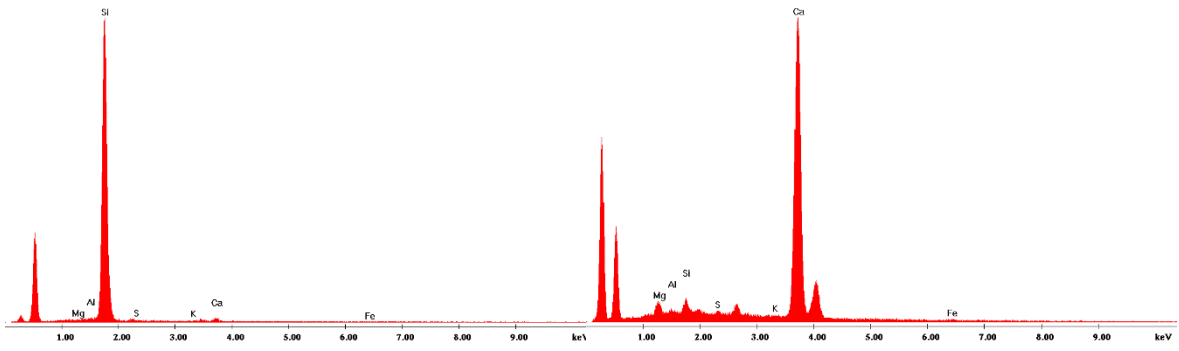


Fig. 44 EDS spectrum of the matrix in sample KJ.16.TC5.1/10

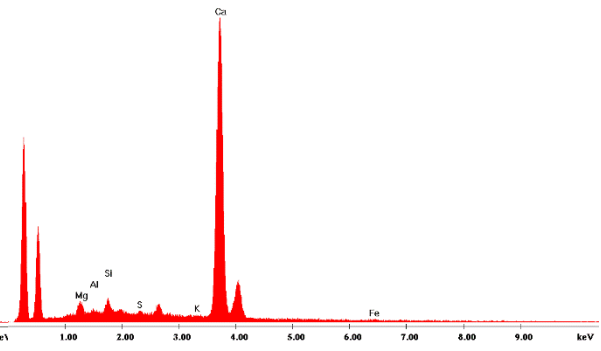
The inclusions in Figure 45 are quartz (point a), iron oxide nodules (point c, e, h), calcareous inclusions (point b, d, f, g) and plagioclase (i).



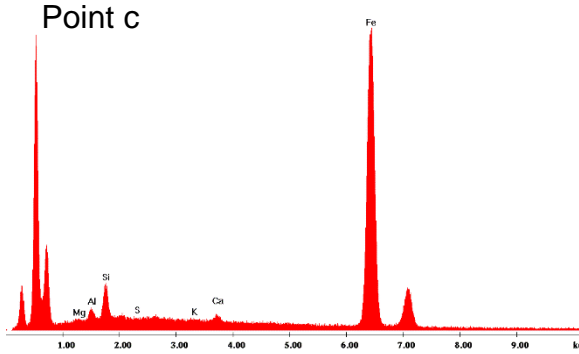
Point a



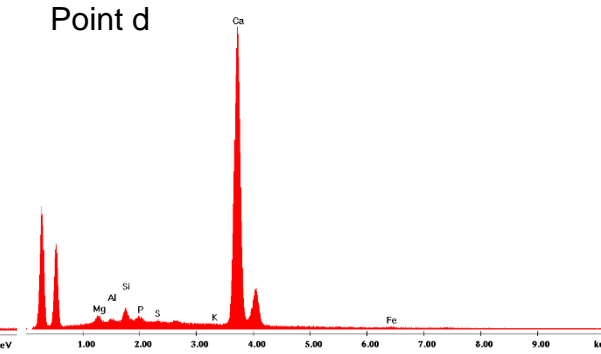
Point b



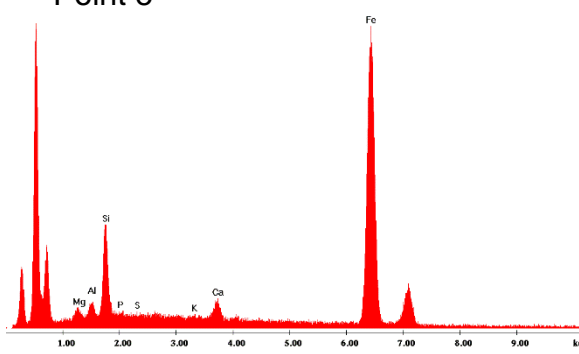
Point c



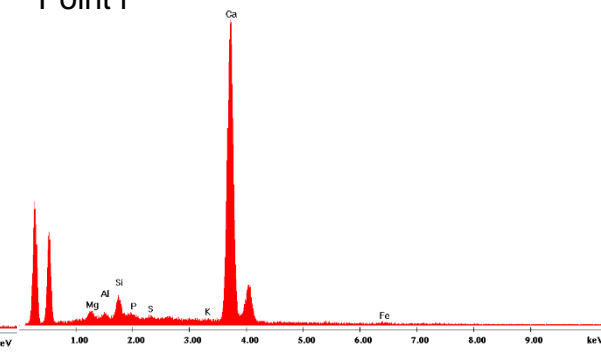
Point d



Point e



Point f



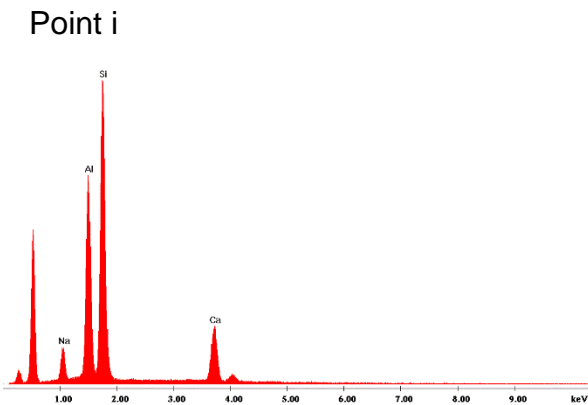
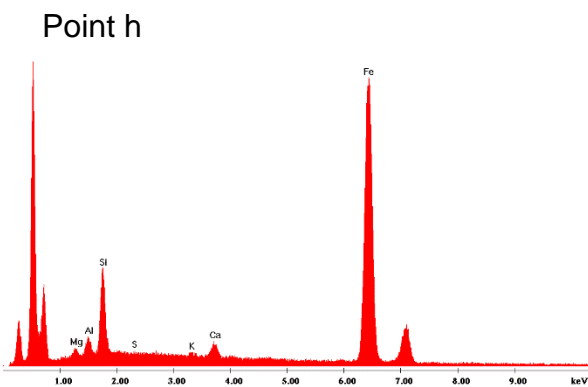
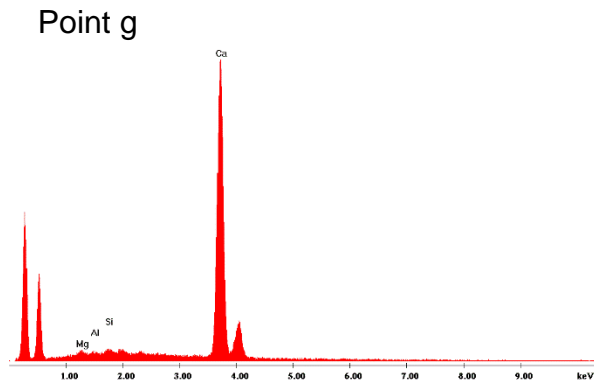


Fig. 45 BSE image and EDS spectra of some marked inclusions in sample KJ.16.TC5.1/10

Figure 46 shows a magnified view of a particular inclusion from the previous image. The calcareous nature of this particle is identified by the high Ca content in all the EDS spectra of Figure 46, except point d, which is characterized by higher Si and lower Ca content.

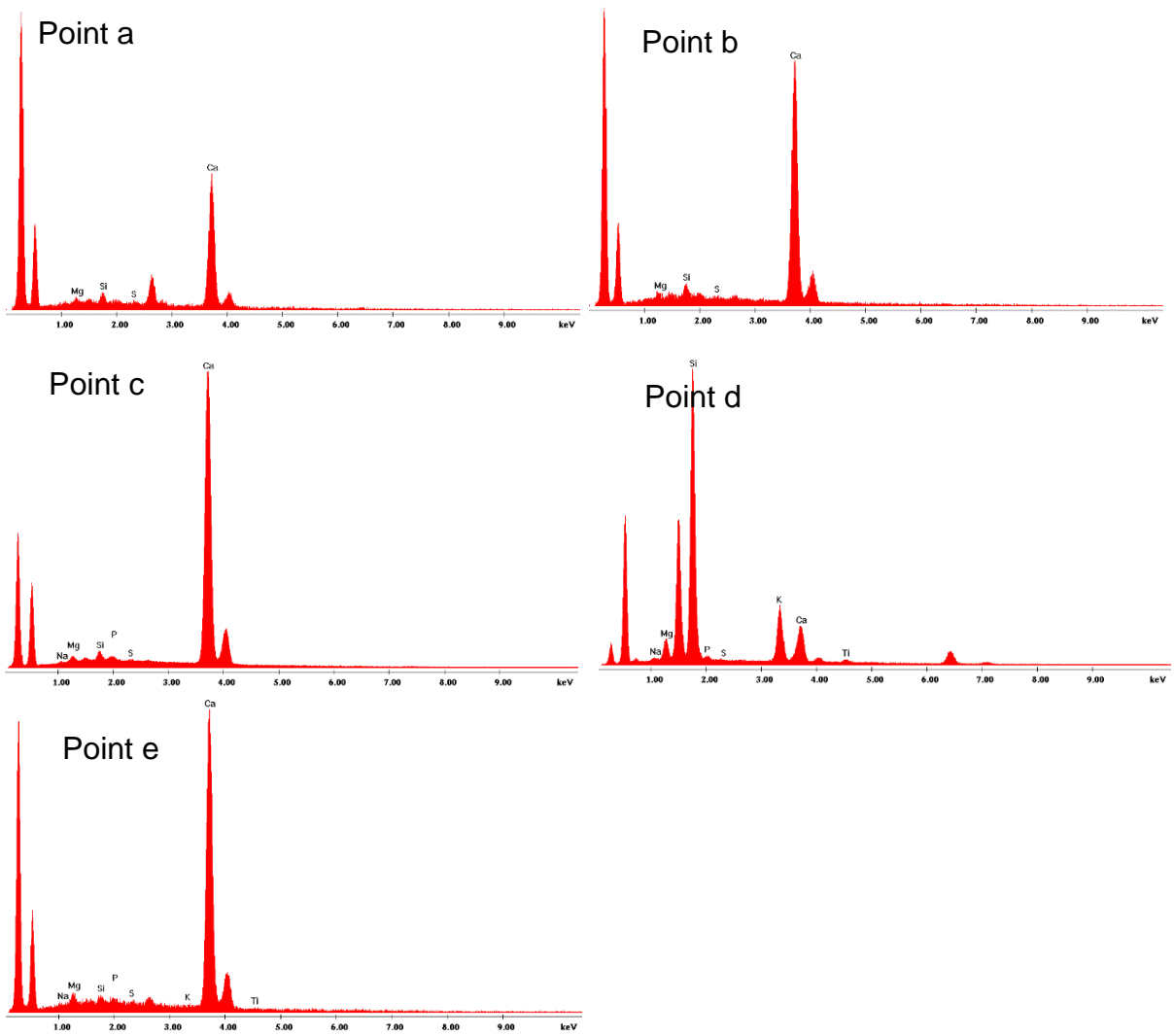
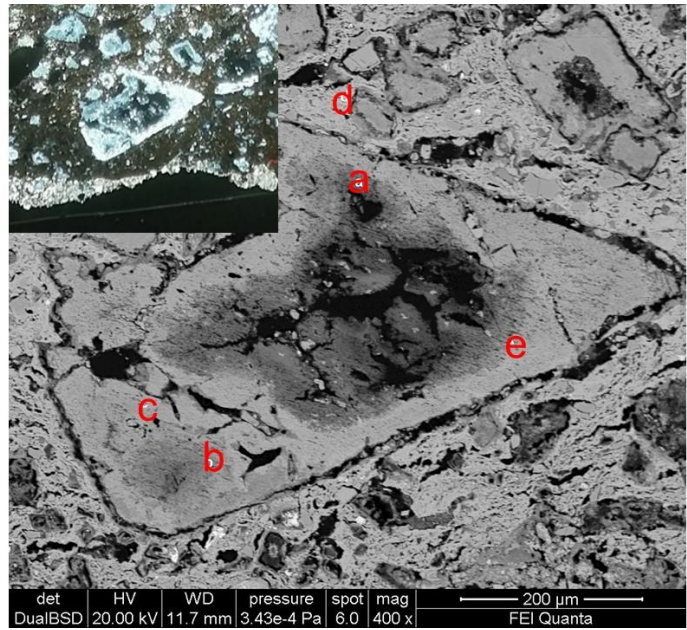


Fig. 46 BSE image of the calcareous inclusions and the spectrum of each point marked inside; the corresponding OM image under XP (top left) is also shown.

Figure 47 is the elemental mapping of the same calcareous inclusion and its surrounding area. Other finer inclusions around are identified by the Ca distribution, while Ca is sporadic in the matrix. Other elements such as Al, Si and K are, contrarily, not found inside the inclusions but relatively abundant in matrix.

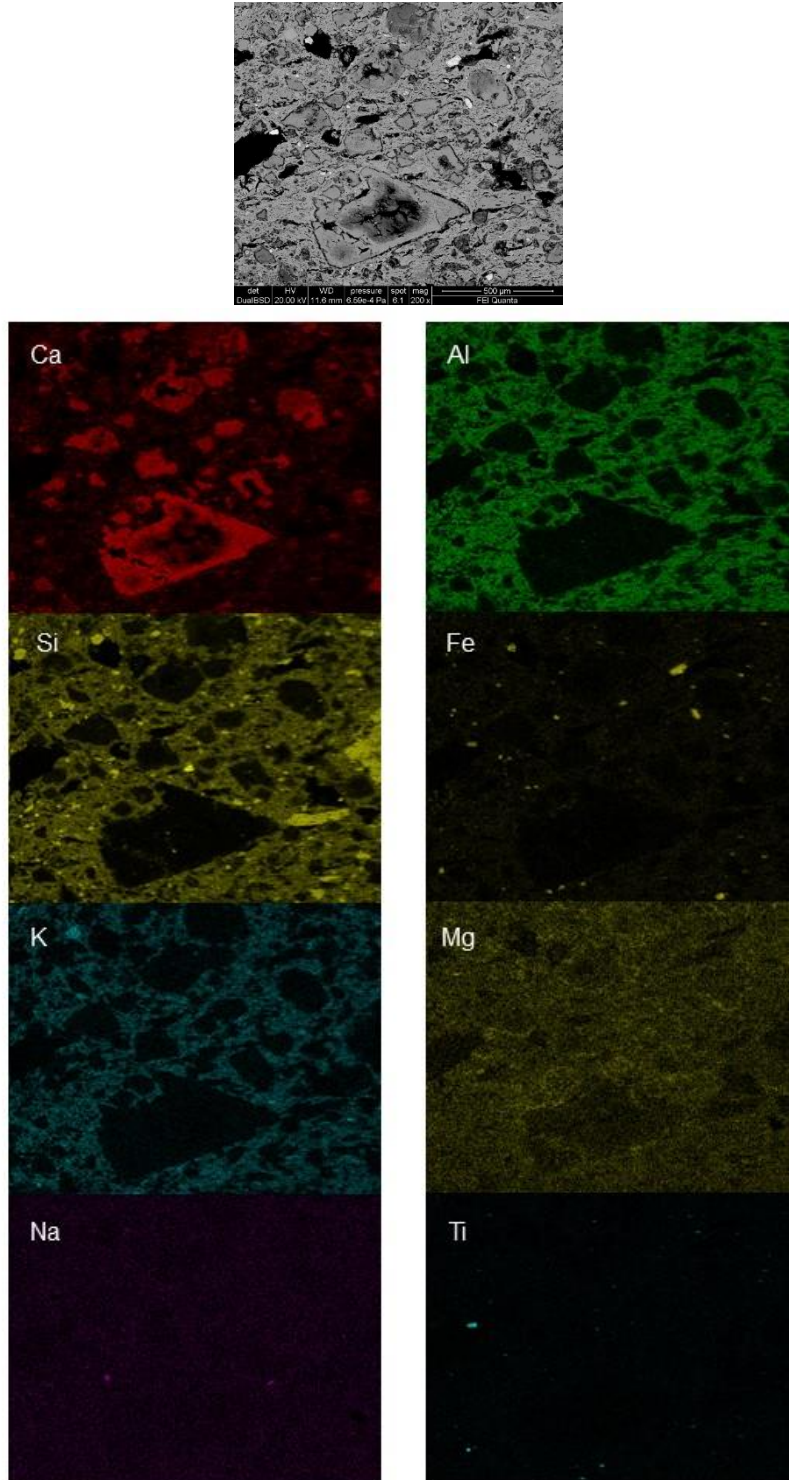


Fig. 47 BSE image and EDS maps of Ca, Al, Si, Fe, K, Mg, Na, Ti of the calcareous inclusion and the area around it.

As in the previous sample, a marginal layer of secondary calcite was found (Fig. 48). The difference in composition of this layer from the matrix is detected and confirmed by the corresponding EDS spectra.

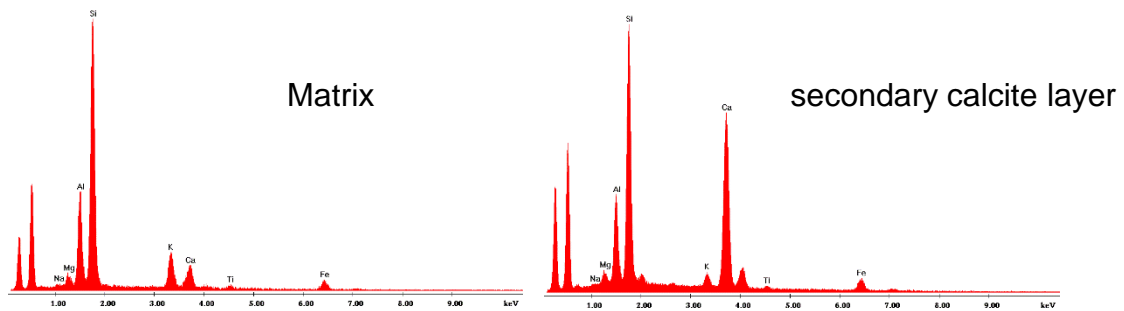
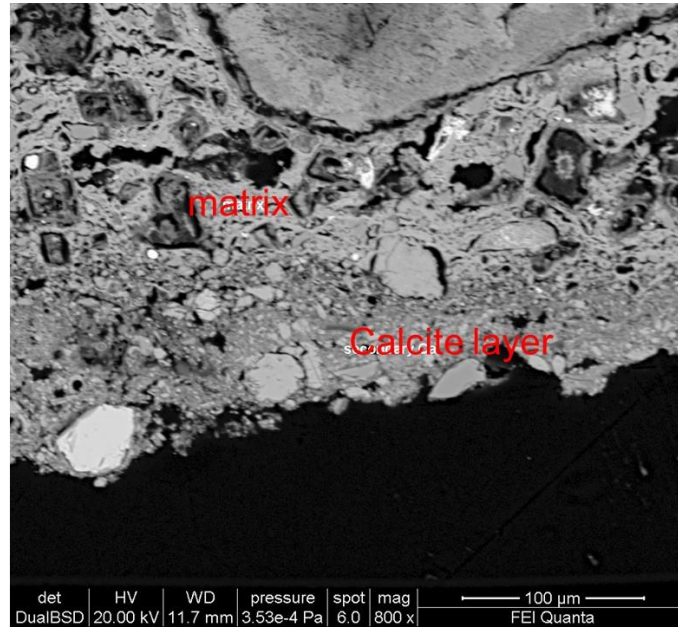


Fig. 48 BSE image and EDS spectra of the matrix (left) and of the secondary calcite layer (right)

This kind of deposition was also documented inside a void and characterized by the EDS spectrum (Fig. 49).

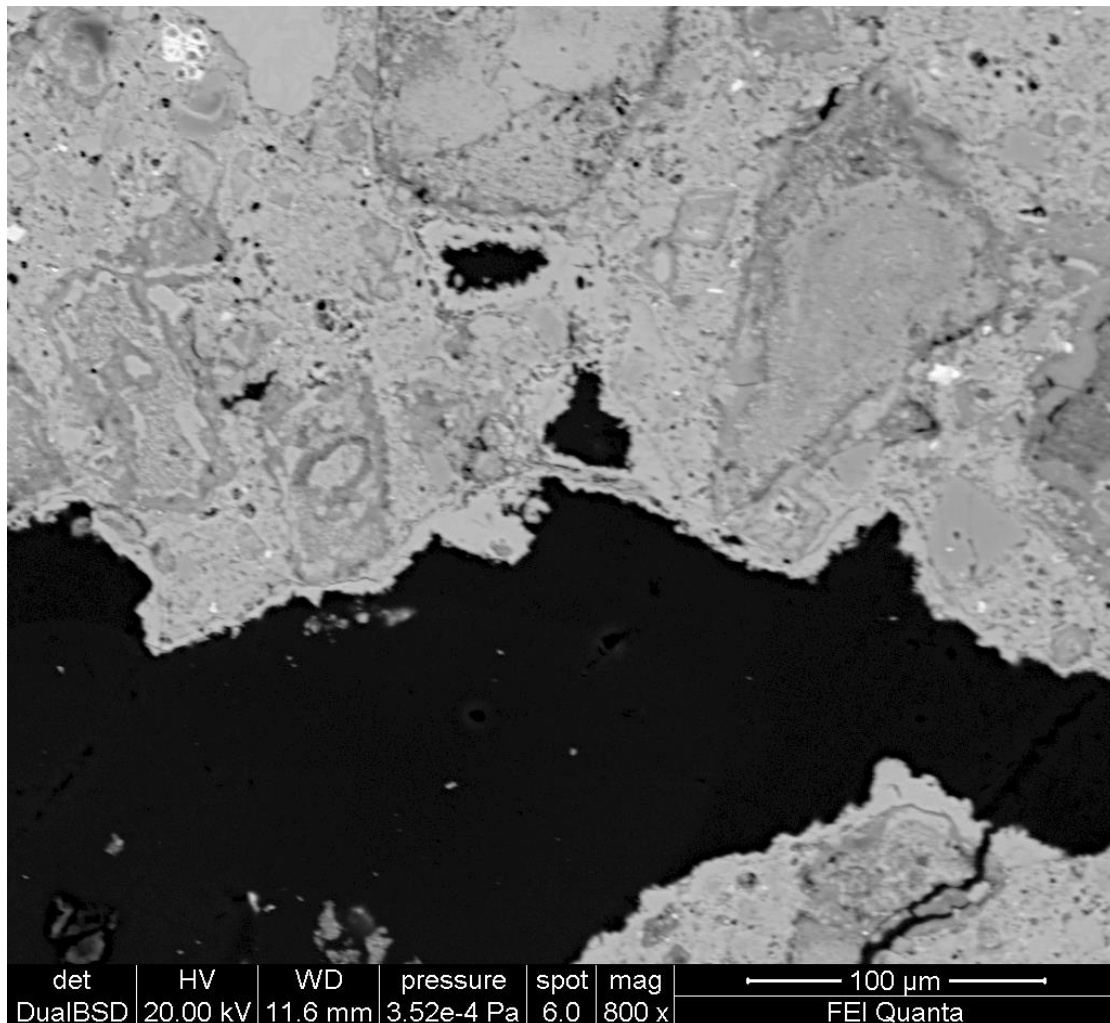


Fig. 49 BSE image and EDS spectrum of a void with secondary calcite inside it.

KJ.16.TC5.1/14

The general spectrum of the matrix is shown in Figure 50. High Si content is detected and minor Al and Ca peaks appear as well. K, Mg, Ti are rarely present.

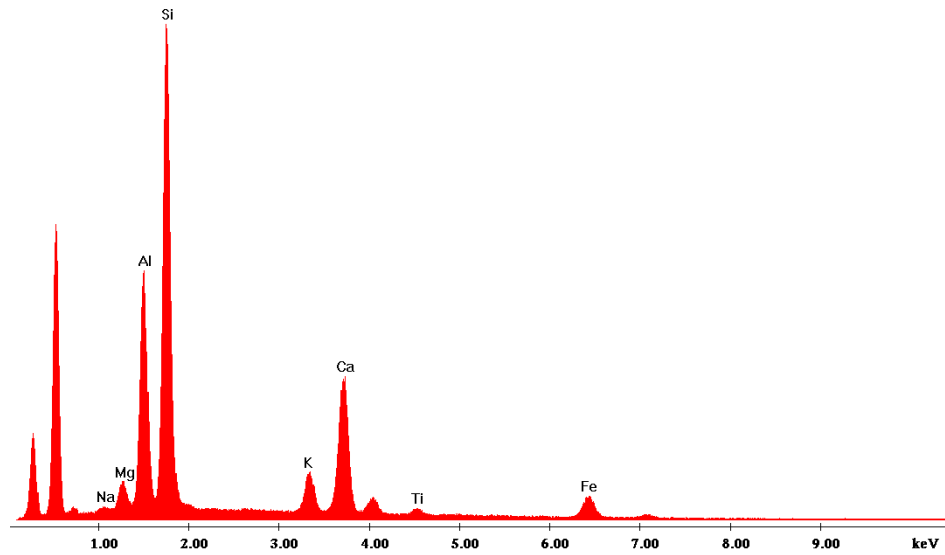


Fig. 50 EDS spectrum from the matrix of sample KJ.16.TC5.1/14

A general mapping was conducted; BSE image and the maps of different elements in a selected area are shown in Figure 51. In most inclusions the core has high amount of both Ca and Mg, while Al, Si and K are abundant in the margins but absent inside the particle core.

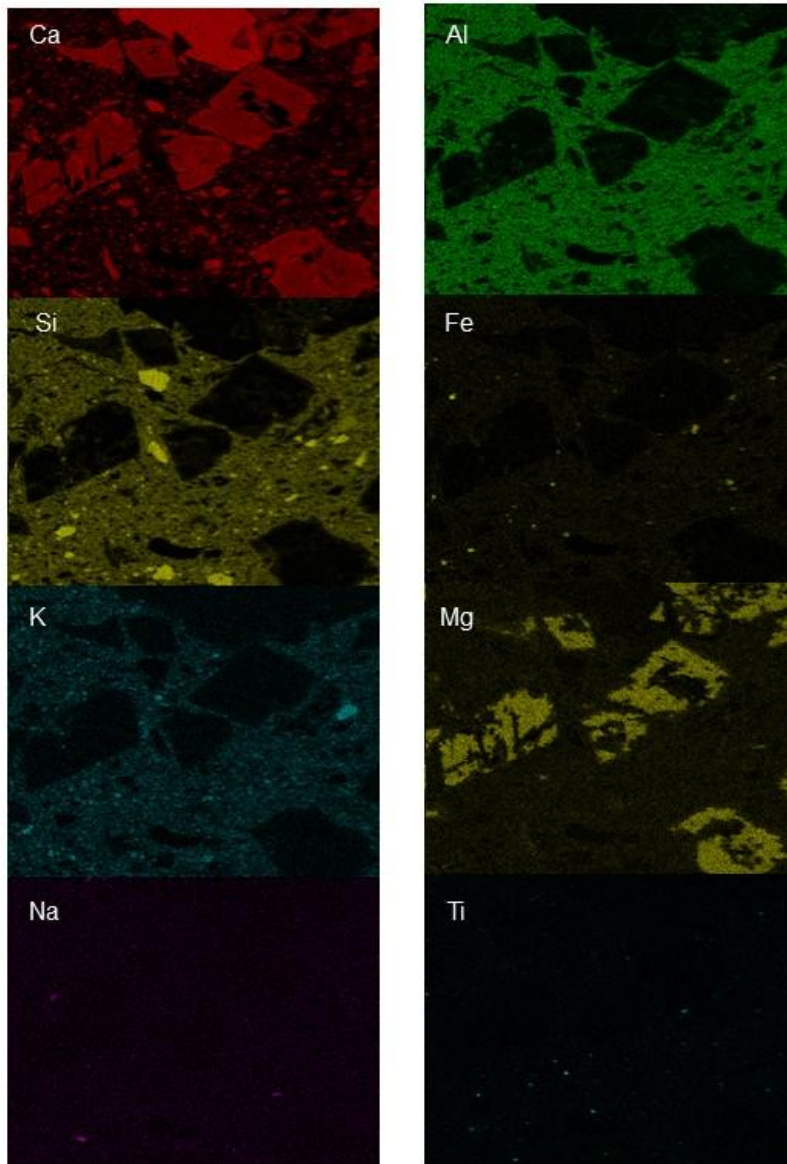
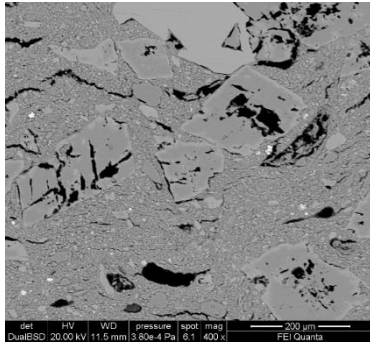


Fig. 51 BSE image and EDS maps of Ca, Al, Si, Fe, K, Mg, Na, and Ti of a chosen area in KJ.16.TC5.1/14

A zoom image of an inclusion with quartz is shown in Figure 52, where the embedded quartz is confirmed by the EDS spectrum of point 2.

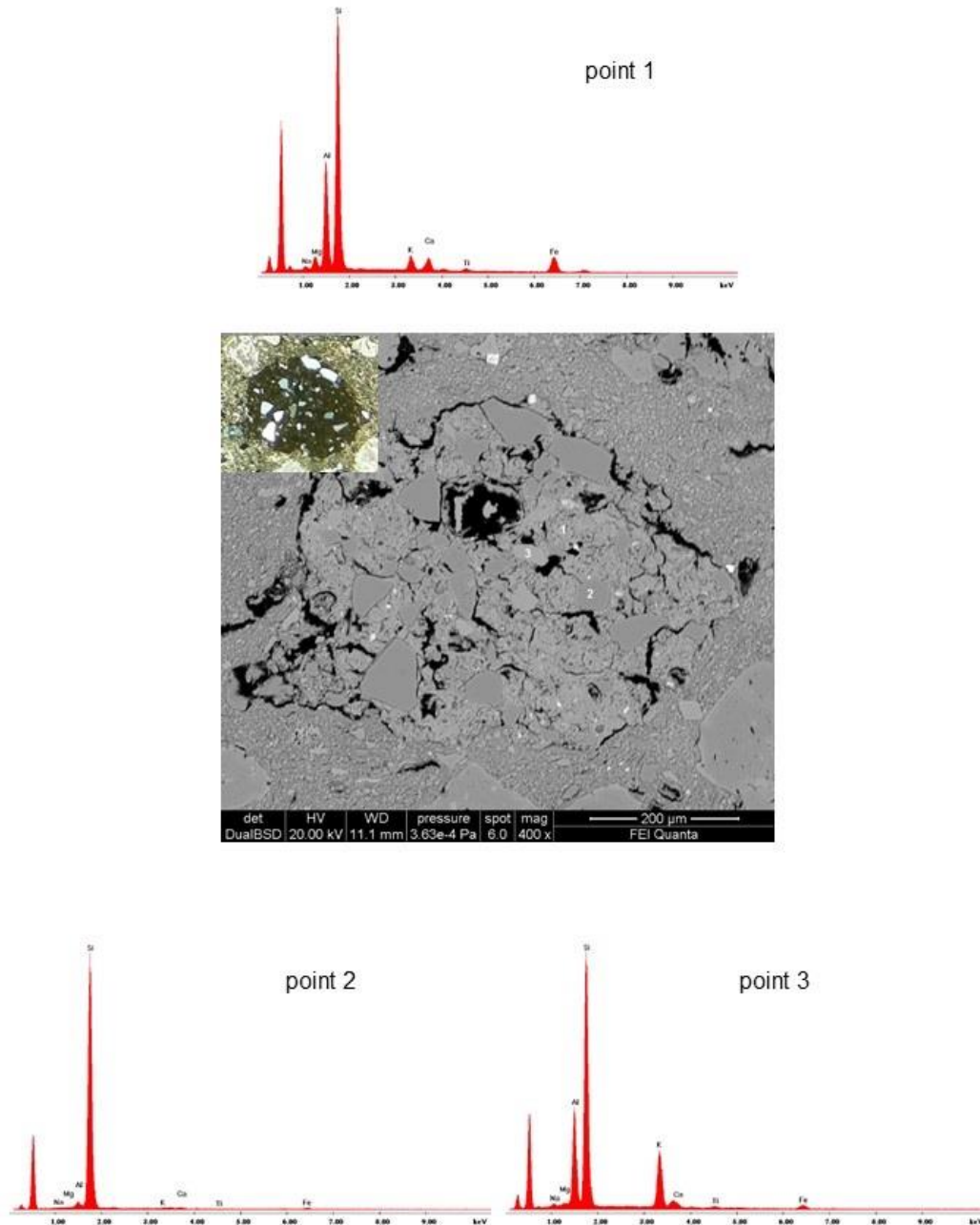


Fig. 52 BSE image and EDS spectra of a few points in a sedimentary rock inclusion with quartz embedded in it, together with the corresponding OM image under XP (top left).

Another inclusion showed to contain dolomite, with Mg and Ca peaks, surrounded by calcite (Fig. 53).

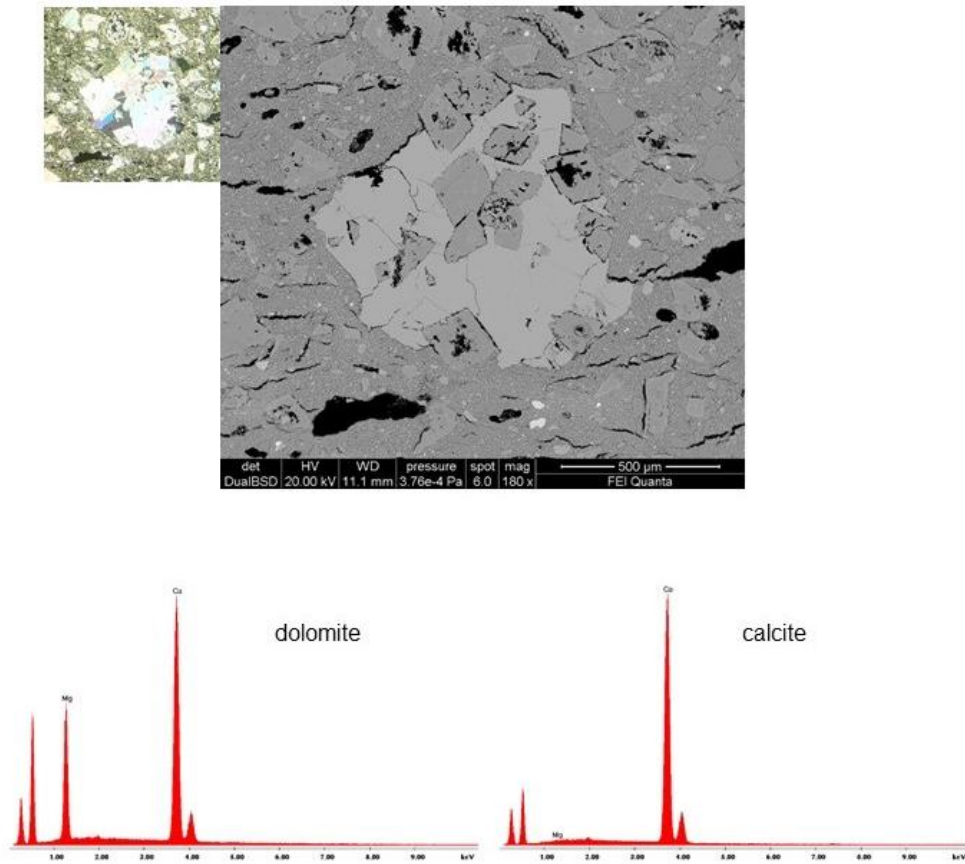


Fig. 53 BSE image and OM image under XP (top left) of dolomite surrounded by calcite, with the spectrum of each mineral

The aggregation of iron oxide nodules is seen here as well, with a final stage and a starting stage (widely distributed iron oxide dots) of the aggregation (Fig. 54).

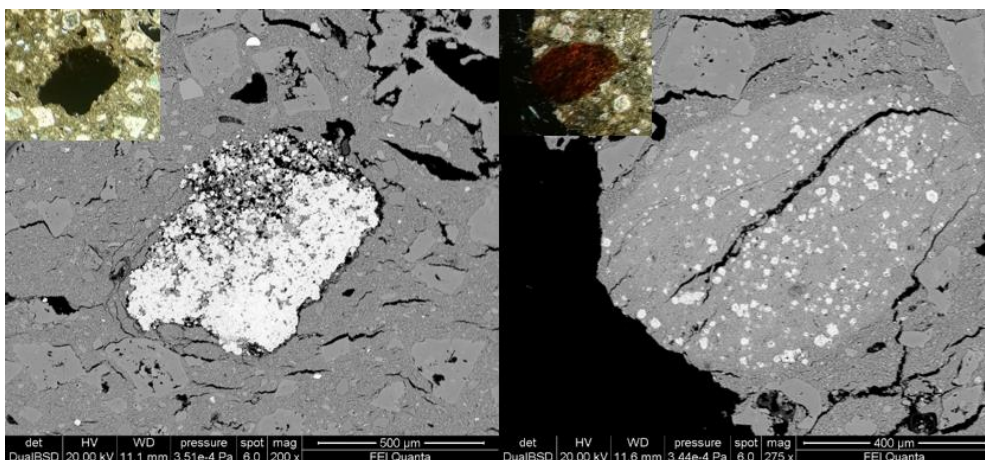


Fig. 54 BSE images, and their corresponding OM image under XP (top left) of two iron oxide nodules at different stages of formation: well-developed stage (left) and starting stage (right)

Chapter 7 Discussion

The study of archaeological ceramics is mainly focused on two aspects: the technological level of the pottery production and the nature as well as the provenance of raw materials (Cultrone *et al.*, 2001; Barone *et al.*, 2002; Sherriff *et al.*, 2002; Maritan & Mazzoli, 2004; Rathossi *et al.*, 2004).

The clay used as raw material and the additive tempers could reflect the desired properties and the functions, as well as the adjustment of workability and firing temperature deliberately decided by ancient potters. Moreover, specific inclusions could reflect the technological skills or preferences of potters of the culture.

Meanwhile, the mineralogical composition of the ceramics could give significant information of the provenance of the raw materials used.

7.1 Technological level

7.1.1 Nature of the raw material

The low number of samples makes it difficult to create petrographic fabrics. However, based on the preliminary results from OM, thus on the nature, percentage and grain size of the inclusions, it is possible to distinguish two groups: the first one includes samples KJ.15.TA7/3 and KJ.16.TC5/1/10 and corresponds to a predominance in fragments of sedimentary calcareous rocks; the other (samples KJ.16.TC5.1/2, KJ.16.TC5/1/3 and KJ.16.TC5/1/14) enriched in calcite and dolomite. In addition to the visible minerals under OM, XRD results revealed the additional presence of other kinds of minerals. The K-feldspar is seen in all samples with a variable amount. Plagioclase, clay minerals, diopside, dolomite, orthopyroxene and wollastonite are found at more than trace amount as well.

To further analyse the matrix, the micro-features of the matrix under SEM-EDS examination are taken into account. The purpose of discerning matrix of these samples is to verify the different clays involved in the ceramic production, which combined with the inclusions features could further give information on the raw materials selection. Here a recognizable basis is the presence or absence of microfossils occurring in the matrix, which give a preliminary separation of clays used. The samples with microfossils are KJ.15.TA7/3, KJ.16.TC5.1/2 and KJ.16.TC5/1/10; the rest two samples KJ.16.TC5/1/3 and KJ.16.TC5/1/14 are hereby categorized as other sort of clay without micro-fossils, thus suggests to be made from clay from different sources. Besides the clay paste, there are significant peculiarities which could be related to decisions in production technology.

Another parameter to infer the technological level achieved by the community in pottery production is the alignment of inclusions and porosity (Tite *et al.*, 2001). The voids in all five samples are generally aligned to the margins, while all inclusions show no alignment. This indicates the probable utilization of manual potter's wheel (i.e. slow wheel or tournette), the extent of kinetic energy being not enough to drive inclusions alignment to the margins as well (Roux, 2009).

The mixing phase can be evaluated by the presence of clay pellets which is not seen in any of the 5 samples under OM, suggesting that the mixing is complete during the production.

The results by OM, XRPD, SEM-EDS analysis allow us to hypothesize the use of a calcareous clay with quartz, feldspars, and fragments of sedimentary calcareous rocks, and whether they are added as temper. This clay is used in all samples, without any apparent relation to particular function or technological reasons, suggesting that probably the use is due to the natural variability in the deposits with micro-fossils.

7.1.2 Firing conditions

The firing conditions in the production process strongly reflect on the final colour of the matrix, which depends on the atmosphere developed within the furnace, the maximum temperature reached, the firing time and the cooling rate (Lofrumento *et al.*, 2004; Molera *et al.*, 1998). The five samples here present mainly a colour tone of reddish or reddish-brown, but still some degree of variability, indicating that the oxygen fugacity was not completely controlled amongst this ceramic firing (Molera *et al.*, 1998).

It is worth mentioning that sample KJ.15.TA7/3 shows a “black core” where the colour changes as a sandwich structure, suggesting that a reducing atmosphere is followed by a cooling stage in oxidizing conditions during the firing process (Medeghini *et al.*, 2016; Nodari *et al.*, 2007).

In addition to the atmosphere, the maximum temperature reached during the firing could be inferred by the nature and state of the mineral inclusions observed in samples (Medeghini *et al.*, 2019).

Clay minerals lose their optical properties completely when temperature reaches 850 °C: the firing temperature was hereby estimated to be lower than this temperature since the general optical activity was still seen in most of the samples. One exception is the sample KJ.16.TC5/1/3 in which no optical activity is observed, thus suggesting a firing temperature higher than 850°C. Moreover, the presence of gehlenite is explained by the starting collapse of clay minerals, following the

reaction (Medeghini & Nigro, 2017):



The trace amount of gehlenite detected in sample KJ.16.TC5/1/3 suggests the initial formation in the temperature range between 800 and 950 °C, which is the range of gehlenite crystallization. The minor abundance in diopside further reduces the range to 850-950°C.

The presence of calcareous inclusions (calcite crystals, limestone fragments, microfossils) could be an indicator of firing temperature as well. In samples KJ.15.TA7/3, KJ.16.TC5/1/2 and KJ.16.TC5/1/14, the presence of calcite suggests a firing temperature lower than the threshold of decarbonation process (Trindade *et al.*, 2009; Bayazit *et al.*, 2014), which is also supported by the absence of gehlenite, indeed the firing is inferred to be done below 800 °C.

In samples KJ.16.TC5/1/3 and KJ.16.TC5/1/10 such alteration is observed, indicating that high temperature destroyed margin alteration and this pottery was fired at a temperature close to the temperature of carbonate/calcite thermal decomposition (800-850°C).

7.2 Provenance

The provenance of raw materials is one of the main aims in the study of ancient pottery. The definition of the mineralogical composition is fundamental to reach this purpose.

Samples unearthed from Khalet al-Jam'a show the use of calcareous clay with quartz, feldspars, and fragments of sedimentary calcareous rocks as inclusions.

Considering the minerals identified, quartz and calcite are not useful to this function since they are common minerals in clay deposit (Papachristodoulou *et al.*, 2006).

Furthermore, some samples present micro-fossils in the matrix, discerning the sort of clays from others. These fossils are identified as planktonic and other benthic foraminifera suggesting that they are from the Lisan formation (Medeghini *et al.*, 2019), thus supporting the hypothesis of a local supply.

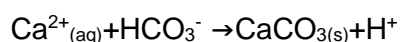
7.3 Burial Conditions

Post-burial processes could be another study topic in addition to the production. The resultant formation of secondary mineral phases, such as gypsum, bassanite, calcite, lepidocrocite and goethite, could be due to the interaction between the ceramics and the burial environment (Heimann & Maggetti 1981; Maggetti, 1982; Freestone, 2001; De Benedetto *et al.*, 2002; Schwedt *et al.*, 2004, 2006; Secco *et al.*, 2011).

The deposition types and kinetics are closely related to the surrounding environment, the characteristics of ceramics (e.g., porosity, texture, mineralogy and chemistry), or any organic substance contacted during the utilization (Freestone, 2001). Parameters affecting and determining the deposition could be temperature cycles, freezing processes, pressure, groundwater composition, acidity, and redox conditions (Freestone, 2001). Among these parameters, groundwater is the main controlling factor which determines the chemical and mineralogical transformations of ceramics by dissolution, alteration and/or precipitation of secondary mineral phases, that could take place on the surface or through pores inside the sherds (Schwedt *et al.*, 2004, 2006; Secco *et al.*, 2011).

In this study, these phenomena were observed in samples KJ.15.TA7/3 and KJ.16.TC5/1/10, the secondary calcite deposition layer found on the surface and, in the latter, also in the pores inside the ceramics. This could infer a mineralization alteration resulting from the burial environment or condition along the surface and contour of the pores (Freestone, 2001), since the porosity allowed the soil to immerse into the voids and deposit on the surface.

The basic required condition for the precipitation of secondary calcite from the solution at standard concentrations of calcium and hydrogen carbonate are according to the reaction (Secco *et al.*, 2011):



This constraint provides the probable conditions (Krumbein & Garrels, 1952) of the burial environment: pH>7 and Eh<-0.2 V.

Chapter 8 Conclusions

The study of five chosen ceramic samples from the Khalet al-Jam'a site, is undertaken by means of mineralogical-petrographic and chemical characterization of these potsherds. By optical and electron microscope, two different clays were distinguished based on the presence/absence of micro-fossils. Those made of clay with fossils are samples KJ.15.TA7/3, KJ.16.TC5.1/2 and KJ.16.TC5/1/10; the rest two samples, KJ.16.TC5/1/3 and KJ.16.TC5/1/14, are hereby categorized as other sort of clay without micro-fossils. Another grouping is done based on the preliminary OM observation: the first group includes samples KJ.15.TA7/3 and KJ.16.TC5/1/10, with a predominant composition of fragment of sedimentary calcareous rocks while the other group (samples KJ.16.TC5.1/2, KJ.16.TC5/1/3 and KJ.16.TC5/1/14) is enriched in calcite and dolomite. To further infer the technological level achieved in the community, the alignment of inclusions and porosity were taken into consideration. A common feature is found: the pores in all samples are generally aligned to the margins, while all inclusions show no alignment, suggesting that the production was probably conducted by manual potter's wheel.

The firing atmosphere was first identified by the colour of the potsherds, from which all the samples are assumed to be fired in uncontrolled atmosphere conditions. Additionally, the black core structure observed in sample KJ.15.TA7/3 indicated a more complicated firing process and that the redox atmosphere changed during the firing. The maximum firing temperature is assumed to fall into the range of 850-950°C, based on the minerals observed in sample KJ.16.TC5/1/3. Other samples such as KJ.16.TC5/1/2 and KJ.16.TC5/1/14 are below 800°C, while samples KJ.16.TC5/1/3 and KJ.16.TC5/1/10 are assumed to be fired at a range of 800-850°C.

The provenance study came to the conclusion that raw materials were probably from the local geological area, identified by the clays, inclusions and micro-fossils coming from local limestones and marls.

Secondary burial alteration is observed in samples KJ.15.TA7/3 and KJ.16.TC5/1/10, in which a secondary calcite deposit layer is found along the surface, but also at the contour of inner pores. This may indicate a certain burial condition with a specific pH value of the surrounding or groundwater.

The technological level and the provenance provide some degree of the understanding, as well as to peek into the past socio-economic systems of production and consumption of the ceramics in ancient Bethlehem.

References

- al-Jam'a, K. (2015). A Middle Bronze and Iron Age necropolis near Bethlehem (Palestine). *Vicino Oriente*, 185-218.
- Applied Research Institute Jerusalem, Environmental Profile for the West Bank, Bethlehem District. (1995).
- Barone, G., Ioppolo, S., Majolino, D., Migliardo, P., & Tigano, G. (2002). A multidisciplinary investigation on archaeological excavation in Messina (Sicily). Part I: a comparison of pottery findings in "the Strait of Messina area". *Journal of Cultural Heritage*, 3(2), 145-153.
- Bayazit, M., Işık, I., Issi, A., & Genç, E. (2014). Spectroscopic and thermal techniques for the characterization of the first millennium AD potteries from Kuriki-Turkey. *Ceramics International*, 40(9), 14769-14779.
- Brindley, G. W. (1980). Crystal structures of clay minerals of clay minerals and their X-ray identification. *Mineralogical Society Monograph.*, 5, Chapter-2.
- Burdon D.J. (1959): Government of the Hashemite Kingdom of Jordan, pp. 82
- Chen Kelun. (2004). *Chinese Porcelain: Art, Elegance, and Appreciation*. Long River Press.
- Cultrone, G., Rodriguez-Navarro, C., Sebastian, E., Cazalla, O., & De La Torre, M. J. (2001). Carbonate and silicate phase reactions during ceramic firing. *European Journal of Mineralogy*, 13(3), 621-634.
- De Benedetto, G. E., Laviano, R., Sabbatini, L., & Zambonin, P. G. (2002). Infrared spectroscopy in the mineralogical characterization of ancient pottery. *Journal of Cultural Heritage*, 3(3), 177-186.
- Diamond, J. (1998). Japanese roots. *Discover*, 19(6), 86-94.
- Finlay, R. (1998). The pilgrim art: The culture of porcelain in world history. *Journal of World History*, 141-187.
- Freestone, I. C. (2001). Post-depositional changes in archaeological ceramics and glasses. *Handbook of archaeological sciences*, 615-625.
- Ghanem, M., Samhan, S., Carlier, E., & Ali, W. (2011). Groundwater pollution due to pesticides and heavy metals in North West Bank.
- Grim, R. E. (1962). Applied Clay Mineralogy. McGraw-Hill Book Company. *New York, USA*.
- Heimann, R. B., & Maggetti, M. (1981). Experiments on simulated burial of calcareous Terra Sigillata (mineralogical change). Preliminary results. In *Scientific studies in ancient ceramics* (Vol. 19, pp. 163-177).
- Huysecom, E., Rasse, M., Lespez, L., Neumann, K., Fahmy, A., Ballouche, A., Ozainne, S., Maggetti, M., Tribolo, Ch. & Soriano, S. (2009). The emergence of

- pottery in Africa during the tenth millennium cal BC: new evidence from Ounjougou (Mali). *Antiquity*, 83(322), 905-917.
- Kramer, S. N. (2010). *The Sumerians: Their history, culture, and character*. University of Chicago Press.
- Krumbein, W. C., & Garrels, R. M. (1952). Origin and classification of chemical sediments in terms of pH and oxidation-reduction potentials. *The Journal of Geology*, 60(1), 1-33.
- Lofrumento, C., Zoppi, A., & Castellucci, E. M. (2004). Micro-Raman spectroscopy of ancient ceramics: a study of French sigillata wares. *Journal of Raman Spectroscopy*, 35(8-9), 650-655.
- Maggetti, M. (1982). Phase analysis and its significance for technology and origin. In *Archaeological ceramics* (pp. 121-133).
- Maritan, L., & Mazzoli, C. (2004). Phosphates in archaeological finds: implications for environmental conditions of burial. *Archaeometry*, 46(4), 673-683.
- Medeghini, L., & Nigro, L. (2017). Khirbet al-Batrawy ceramics: a systematic mineralogical and petrographic study for investigating the material culture. *Periodico di Mineralogia*, 86, 19-35.
- Medeghini, L., Mignardi, S., De Vito, C., Macro, N., D'Andrea, M., & Richard, S. (2016). New insights on Early Bronze Age IV pottery production and consumption in the southern Levant: The case of Khirbat Iskandar, Jordan. *Ceramics International*, 42(16), 18991-19005.
- Medeghini, L., Sala, M., De Vito, C., & Mignardi, S. (2019). A forgotten centre of ceramic production in Southern Levant: Preliminary analytical study of the Early Bronze Age pottery from Tell el-Far 'ah North (West Bank). *Ceramics International*, 45(9), 11457-11467.
- Meyer, M., Daszkiewicz, M., Schneider, G., Bernbeck, R., Heeb, B. S., Hegewisch, M., Kohlmeyer, K., Näser, C., Polla, S., Schultze, E., Schweigart, F. & Warburton, D. A. (2016). Economic Space: On the Analysis and Interpretation of Pottery Production and Distribution. *J. Ancient Studies, Special Volume: Space and Knowledge. Topoi Research Group Articles*, 190–219.
- Molera, J., Pradell, T., & Vendrell-Saz, M. (1998). The colours of Ca-rich ceramic pastes: origin and characterization. *Applied Clay Science*, 13(3), 187-202.
- Nesse, W. D. (2012). *Introduction to mineralogy* (No. 549 NES).
- Nigro, L., Montanari, D., Guari, A., Tamburrini, M., Izzo, P., Ghayyada, M., Titi, I., Yasmine, J. (2017). New archaeological features in Bethlehem (Palestine): the Italian-Palestinian rescue season of 2016, *VICINO ORIENTE XXI*, 5-57

- Nigro, L., Montanari, D., Ghayyada, M., & Yasmine, J. (2018). Protecting and rehabilitating the archaeology of Bethlehem. *Antiquity*, 92(365), 1-7.
- Nodari, L., Marcuz, E., Maritan, L., Mazzoli, C., & Russo, U. (2007). Hematite nucleation and growth in the firing of carbonate-rich clay for pottery production. *Journal of the European Ceramic Society*, 27(16), 4665-4673.
- Papachristodoulou, C., Oikonomou, A., Ioannides, K., & Gravani, K. (2006). A study of ancient pottery by means of X-ray fluorescence spectroscopy, multivariate statistics and mineralogical analysis. *Analytica Chimica Acta*, 573, 347-353.
- Rathossi, C., Tsolis-Katagas, P., & Katagas, C. (2004). Technology and composition of Roman pottery in northwestern Peloponnese, Greece. *Applied Clay Science*, 24(3-4), 313-326.
- Rado, P. (1988). An introduction to the technology of pottery.
- Reedy, C. L. (2008). *Thin-section petrography of stone and ceramic cultural materials*. London: Archetype.
- Roux, V. (2009). Wheel Fashioned Ceramic Production during the Third Millennium BCE in the Southern Levant : a Perspective from Tel Yarmuth. Rosen Steven A., Roux Valentine *Techniques and people : anthropological perspectives on technology in the archaeology of the proto-historic and early historic periods in the Southern Levant*, de Boccard, pp.195-212, 2009, Mémoires et travaux du Centre de recherche français à Jérusalem, 978-2701802695.
- Wheel fashioned ceramic production during the third millennium BCE in the Southern Levant: a perspective from Tel Yarmuth.
- Saleh, A., Neiroukh, F., Ayyash, O., & Gasteyer, S. (1995). Pesticide usage in the West Bank. *Applied Research Institute-Jerusalem (ARIJ)*, 22.
- Schwedt, A., Mommsen, H., & Zacharias, N. (2004). Post-depositional elemental alterations in pottery: neutron activation analyses of surface and core samples. *Archaeometry*, 46(1), 85-101.
- Schwedt, A., Mommsen, H., Zacharias, N., & Garrigós, J. B. I. (2006). Analcime crystallization and compositional profiles—comparing approaches to detect post-depositional alterations in archaeological pottery. *Archaeometry*, 48(2), 237-251.
- Secco M., Maritan L., Mazzoli C., Lampronti G.I., Zorzi F., Nodari L., Russo U., Mattioli S.P. (2011): Alteration processes of pottery in lagoon-like environments. *Archaeometry*, 53 (4), 809-829
- Selkirk, R. (2003). The Oldest Pottery in the World. *Current World Archaeology*. pp. 44–49
- Shalash, I., & Ghanem, M. (2008). Hydrochemistry of the Natuf drainage basin in Ramallah area/West Bank. *Environmental geology*, 55(2), 359-367.

- Sherriff, B. L., Court, P., Johnston, S., & Stirling, L. (2002). The source of raw materials for Roman pottery from Leptiminus, Tunisia. *Geoarchaeology: An International Journal*, 17(8), 835-861.
- Sillar, B. (1997). WILLIAM K. BARNETT & JOHN W. HOOPES (ed.). The emergence of pottery: Technology and innovation in ancient societies. xviii 285 pages, 71 illustrations, 17 tables. 1995. Washington [DC]: Smithsonian Institution Press; *Antiquity*, 71(272), 494-497.
- Sinopoli, C. M. (1991). Approaches to archaeological ceramics. In *Approaches to Archaeological Ceramics* (pp. 1-7). Springer, Boston, MA.
- Trindade, M. J., Dias, M. I., Coroado, J., & Rocha, F. (2009). Mineralogical transformations of calcareous rich clays with firing: a comparative study between calcite and dolomite rich clays from Algarve, Portugal. *Applied Clay Science*, 42(3-4), 345-355.
- Tite, M. S., Kilikoglou, V., & Vekinis, G. (2001). Strength, toughness and thermal shock resistance of ancient ceramics, and their influence on technological choice. *Archaeometry*, 43(3), 301-324.
- Vandiver, P. B., Soffer, O., Klima, B., & Svoboda, J. (1989). The origins of ceramic technology at Dolní Věstonice, Czechoslovakia. *Science*, 246(4933), 1002-1008.
- Whitbread, I. K. (1986). The characterisation of argillaceous inclusions in ceramic thin sections. *Archaeometry*, 28(1), 79-88.
- Whitbread, I. K. (1995). *Greek transport amphorae: a petrological and archaeological study*.

Acknowledgement

I would first like to thank my thesis advisor Dott.ssa Laura Medeghini of Dept. of Earth Sciences at Sapienza University of Rome. From the very beginning of the thesis work, she gave every reference and background information of the frame of the work, and helped me with the most difficult sampling part.

Throughout the laboratory work, she considerably helped me with every single detail and techniques of the devices. Whenever I ran into a trouble spot or had a question about my research or writing, she always gave me kindly advice, and check every detail of the thesis work for me throughout the whole process.

I would also like to thank Dott.ssa Michela Botticelli, who accompanied with us during the SED experiment part, and kindly gave me advice and expertise on the interpretation of this part, which is the most complicated part among all techniques.

I would also like to acknowledge Prof. Silvano Mignardi of Dept. of Earth Sciences, he graciously helped me with the final checking of my thesis writing and made it in better version.

Finally, I must express my very profound gratitude to my parents and to all ARCHMATians, especially those in Rome, for providing me with unfailing support and encouragement throughout my years of study and made it a amazing and Unforgettable adventure. This accomplishment would not have been possible without them. Thank you.

Yun-Wen Liao